

26  
7-8-80  
23  
SAND 80-0709  
Unlimited Release

THERMAL PROPERTIES MEASUREMENT ON ROCKSALT  
SAMPLES FROM THE SITE OF THE PROPOSED WASTE  
ISOLATION PILOT PLANT

MASTER

J. N. Sweet and J. E. McCreight

Prepared by Sandia Laboratories, Albuquerque, New Mexico 87185  
and Livermore, California 94550 for the United States Department of  
Energy under Contract AT(29-1)-789

May 13, 1980



Sandia National Laboratories

## **DISCLAIMER**

**This report was prepared as an account of work sponsored by an agency of the United States Government. Neither the United States Government nor any agency Thereof, nor any of their employees, makes any warranty, express or implied, or assumes any legal liability or responsibility for the accuracy, completeness, or usefulness of any information, apparatus, product, or process disclosed, or represents that its use would not infringe privately owned rights. Reference herein to any specific commercial product, process, or service by trade name, trademark, manufacturer, or otherwise does not necessarily constitute or imply its endorsement, recommendation, or favoring by the United States Government or any agency thereof. The views and opinions of authors expressed herein do not necessarily state or reflect those of the United States Government or any agency thereof.**

## **DISCLAIMER**

**Portions of this document may be illegible in electronic image products. Images are produced from the best available original document.**

Issued by Sandia Laboratories, operated for the United States  
Department of Energy by Sandia Corporation.

---

**NOTICE**

This report was prepared as an account of work sponsored by the United States Government. Neither the United States nor the Department of Energy, nor any of their employees, nor any of their contractors, subcontractors, or their employees, makes any warranty, express or implied, or assumes any legal liability or responsibility for the accuracy, completeness or usefulness of any information, apparatus, product or process disclosed, or represents that its use would not infringe privately owned rights.

Printed in the United States of America

Available from  
National Technical Information Service  
U.S. Department of Commerce  
5285 Port Royal Road  
Springfield, VA 22161

Price: Printed Copy \$5.25; Microfiche \$3.00

THERMAL PROPERTIES MEASUREMENTS ON ROCKSALT SAMPLES FROM THE SITE OF THE  
PROPOSED WASTE ISOLATION PILOT PLANT

J. N. Sweet and J. E. McCreight  
Thermophysical Properties Division

Abstract

Thermal conductivity, thermal expansion, and specific heat measurements have been made on a number of specimens cut from core samples obtained from drill holes at or near the site of the proposed Waste Isolation Pilot Plant (WIPP). The specific heat measurements were made by differential scanning calorimetry and the results showed that the specific heats of both clean rocksalt samples and of dirty samples with  $\leq 7\%$  insoluble impurities were essentially identical to the published specific heat for pure NaCl. In the thermal expansion measurements, two distinct groups of samples were identified. The first group had average expansion coefficients in the temperature range 300-700 K close to that reported for pure NaCl. All the samples in this group were composed predominantly of halite, with only small amounts of other minerals or materials present. A second group of samples had expansion coefficients only  $\sim 0.3$ - $0.5$  that of NaCl. The samples in this group were composed largely of polyhalite, anhydrite, or siltstone.

The measurements first reported by Acton on the thermal conductivity of samples taken from a borehole at the site of the proposed nuclear waste isolation pilot plant (WIPP) near Carlsbad, NM, have been extended to include additional samples and higher temperature measurements. Samples for these measurements were taken from several depths of three wells, including the well AEC 8 from which Acton obtained his samples. These samples ranged from relatively pure rocksalt (NaCl) with small amounts of interstitial anhydrite to essentially nonsalt samples composed of gypsum or clay. The measurements in this latest series were conducted at Sandia using the longitudinal heat flow apparatus described by Acton, at the Los Alamos Scientific Laboratory (LASL) using a transient line source technique, and at Dynatech Corp., Cambridge, MA using a linear heat flow comparative technique.

In general, the data from the three laboratories agreed reasonably well for similar coarse grained translucent rock salt samples, with the LASL and Sandia results typically being about 20% higher than those of Dynatech. The measured rocksalt conductivities in the temperature range 300-700 K are described relatively accurately by an expression of the form,  $\lambda = \lambda_0 (300/T)^\gamma$ , where  $\lambda_0$  = conductivity at 300 K,  $\gamma = 1.14$ , and  $T$  is the temperature in K. The Sandia and LASL data are best described by  $\lambda_0 = 6$  W/m-K, while for the Dynatech data,  $\lambda_0 = 5$  W/m-K yields the best fit. Slack has proposed that a two parameter expression of the form given above for  $\lambda$  is generally applicable to a wide variety of nonmetallic solids, with the deviation of  $\gamma$  from one resulting from both thermal expansion effects and optic-acoustic phonon interactions which are not included in the standard analysis of thermal conductivity caused by phonon transport. The data in the range  $T \geq 500$  K frequently deviates by  $\sim \pm 15\%$  from that predicted by the above functional form.

DISCLAIMER

This book was prepared as an account of work sponsored by an agency of the United States Government. Neither the United States Government nor any agency thereof, nor any of their employees, makes any warranty, express or implied, or assumes any legal liability or responsibility for the accuracy, completeness, or usefulness of any information, apparatus, product, or process disclosed, or represents that its use would not infringe privately owned rights. Reference herein to any specific commercial product, process, or service by trade name, trademark, manufacturer, or otherwise, does not necessarily constitute or imply its endorsement, recommendation, or favoring by the United States Government or any agency thereof. The views and opinions of authors expressed herein do not necessarily state or reflect those of the United States Government or any agency thereof.

DISTRIBUTION OF THIS DOCUMENT IS UNLIMITED

This is not believed to be the result of the onset of radiative thermal transport because the deviations are negative as well as positive. Infrared transmission measurements on rocksalt samples from the proposed WIPP site show no transmission in the 3-10  $\mu\text{m}$  wavelength range for samples  $\geq 5$  cm thick. Use of the estimated infrared absorption coefficient leads to the conclusion that there is little radiative heat transport for  $T \leq 800$  K.

For nonsalt samples from the proposed WIPP site, values of  $\lambda_0$  fall in the range 0.5-3 W/m-K and frequently  $\gamma$  values are in the range  $\gamma < 1$ . All samples were dense with little or no porosity evident. On the basis of these experiments, we have concluded that the thermal conductivity of materials found at the site can be predicted to an accuracy  $\sim \pm 30\%$  from knowledge of the composition and grain size of these materials.

## Table of Contents

	<u>Page</u>
Abstract . . . . .	i
I. Introduction . . . . .	2
II. Specific Heat Measurements . . . . .	5
III. Thermal Expansion Measurements . . . . .	8
IV. Thermal Conductivity Measurements and Sample Analysis . . . . .	12
A. Thermal Conductivity Measurement Techniques . . . . .	12
B. Thermal Conductivity Measurement Results . . . . .	20
C. Theory of Salt Thermal Conductivity and Review of Past Measurements . . . . .	25
D. Conclusions on Thermal Conductivity Measurements . . . . .	36
V. Discussion of Thermal Conductivity Variation and Its Effect on Repository Thermal Analysis . . . . .	37
VI. Discussion and Conclusions . . . . .	46
References . . . . .	47
Appendix A - Dynatech Thermal Expansion Report . . . . .	51
Appendix B - Dynatech Thermal Conductivity Report . . . . .	55



## I. Introduction

The purpose of this report is to present and discuss thermal properties measurements made in support of studies of the proposed Waste Isolation Pilot Plant (WIPP). The properties measured were thermal expansion, thermal conductivity, and specific heat. In the case of the thermal conductivity measurements, a brief description of the results and their use in repository thermal analysis has already been given elsewhere.<sup>1</sup> This report contains a more complete description of the conductivity experiments than does Ref. 1 and also includes a section reviewing the theory of salt thermal conductivity. The results of thermal expansion and specific heat measurements are also presented and discussed.

Samples for all the measurements were taken from three drill holes which were designated AEC#8, ERDA#9 and WIPP#19.<sup>2</sup> ERDA#9 is located about 0.1 km from the center of the proposed WIPP site and in a square area approximately 0.6 km on a side designated as zone I-surface facilities area. WIPP#19 is located about 0.9 km north of ERDA#9 in an area over the prospective underground repository, and AEC#8 is located about 6 km northeast of the center and outside the WIPP site boundary. The precise locations of these drill holes are shown in Fig. 2-10 of Ref. 2.

The thermal expansion measurements and most of the conductivity measurements were performed by Dynatech Corp. of Cambridge, Mass. The final Dynatech reports are included as appendices to this report. Some of the thermal conductivity measurements were performed at Sandia as were all of the specific heat measurements. The various core samples were catalogued as to drill hole number and depth, and all of the cores used in the conductivity and expansion experiments were photographed and analyzed qualitatively as to composition by S. J. Lambert of Sandia Laboratories. These photographs are presently maintained on file by the authors of this report. The sample numbers along with the associated well



numbers, depths and descriptions are shown in Table I. An examination of this table shows that most of the samples from the deeper depths were composed primarily of rocksalt or halite ( $\text{NaCl}$ ) and anhydrite ( $\text{CaSO}_4$ ) with polyhalite ( $\text{K}_2\text{Ca}_2\text{Mg}(\text{SO}_4) \cdot 2\text{H}_2\text{O}$ ) and clay as the main additional constituents. Samples from shallower depths contained gypsum and various other materials. Detailed geologic data on mineral composition vs depth at or near the WIPP site is presented in Ref. 2.

As a general result, we found that samples composed primarily of halite and anhydrite had thermal conductivities characteristic of the pure materials. The presence of significant quantities of polyhalite, clay, or rock resulted in a significant lowering of the conductivity. The specific heats of all samples measured had essentially the same magnitude and temperature dependence as that reported for pure halite. In the case of thermal expansion, the samples composed largely of halite had mean coefficients of expansion close to that reported for pure  $\text{NaCl}$ . The presence of significant amounts of anhydrite, polyhalite, or gypsum resulted in a significant lowering of the expansion coefficient.

In the next section, the specific heat measurements are discussed and in Sec. III the thermal expansion measurements are described. In Sec. IV the thermal conductivity measurements are presented and the effect of conductivity variation or uncertainty on repository thermal analysis is investigated in Sec. V. Finally, the major conclusions of this study are set forth in Sec. VI.

Table I. Composition of WIPP Core Samples

The following composite descriptions were given by S. J. Lambert - Div. 4511, Sandia Laboratories.

<u>Core No./ Well No.</u>	<u>Depth (m)</u>	<u>Description</u>
1/AEC#8	825	Coarse grain rocksalt with white interstitial anhydrite (~7%) with fine to coarse grain halite.
2/AEC#8	627	Medium coarse gray rocksalt; fine to very coarse halite with small pockets of gray clay (~2%) and traces of polyhalite (~1/2%).
3/ERDA#9	869	Gray very coarse crystalline rocksalt; medium to very coarse grain halite with wisps of anhydrite (~3%) and interstitial medium gray clay.
4/ERDA#9	589	Contains marker bed number 133. About 2 inches of polyhalite and very fine to coarse grain orange halite. Flesh colored polyhalite.
5/ERDA#9	590	Dense medium red fine grain polyhalite. Marker bed No. 133.
6/ERDA#9	503	Marker bed number 124. Dense gray laminated anhydrite.
7/ERDA#9	336	Medium to very coarse grain orange halite (~4%) with reddish brown clay in wispy stringers (~1%). Polyhalite associated with clay.
8/ERDA#9	607	Coarse to very coarse grain halite with anhydrite (~4%) in irregular clots and stringers, interstitial up to 2 cm long (~3%). Medium gray clay occurring as anhydrite does.
9/AEC#8	610	About 8 inches of dense red polyhalite containing beds of coarse grain halite up to 2 cm thick and grading upward to very coarse grain orange halite.
10/AEC#8	609	Light orange medium to very coarse grain halite with wispy band of polyhalite (~40%) near one end.
11/AEC#8	213	Dense gray anhydrite about half converted to 50% gypsum at one end.
12/AEC#8	370	Dark red medium grain halite (~60%) and red clay (~40%).
13/AEC#8	629	Very coarse grain rocksalt with minimal clay. Traces of anhydrite and very thin line of patchy polyhalite.
14/WIPP#19	188	Dark pink medium grain laminated gypsum.
15/WIPP#19	82	Laminated cross bedded micaceous silt stone with a veinlet of gypsum parallel to bedding near the 268' level about 4 mm thick.

## II. Specific Heat Measurements

All of the samples for specific heat measurements were taken from the ERDA#9 drill hole. The measurements were made with a Perkin-Elmer model DSC-2 differential scanning calorimeter (DSC) over a temperature range 298-700 K. This instrument requires a rather small sample ( $\leq 50$  mg); in order to obtain a sample representative of the bulk, approximately 0.1 kg of each core sample was thoroughly ground to a fine powder. A small sample ( $\sim 50$  mg) of each powder was then scanned on the DSC over the temperature range 298-700 K. The precision of the DSC measurements is estimated to be  $\pm 5\%$ .

In the first series of measurements, no mineral or other geologic information about the samples was recorded. Three core samples were analyzed and the results are shown in Table II.

---

Table II  
Specific Heat Results for Three Core Samples from ERDA#9  
(in kJ/kg-K)

<div>Sample Depth (m)</div> <div>T(K)</div>	<u>673</u>	<u>785</u>	<u>794</u>	<u>NaCl<sup>3</sup></u>
298	0.86	0.87	0.87	0.87
400	0.90	0.90	0.91	0.90
500	0.94	0.95	0.95	0.93
600	0.95	0.95	0.95	0.95
700	0.96	0.97	0.96	0.98

---

The data in the last column of Table II are those reported for pure NaCl<sup>3</sup>. It is evident from inspection of Table II that the three samples used in this experiment

had specific heats very close to that of pure NaCl over the entire temperature range investigated.

In a second series of measurements, the specific heat of a salt sample with a relatively high impurity content (dirty salt) was compared to that of a relatively low impurity content (clean salt). The high impurity sample was selected from a 631 m core section from ERDA#9 and the low impurity sample from a 799 m core. The samples were characterized as follows:

#### Dirty Salt

Appearance: Inclusions of reddish-brown material in a matrix of coarse (~2 cm), clear crystals.

Composition: Soluble-major component of halite (NaCl) with trace of polyhalite ( $K_2Ca_2Mg(SO_4)_4 \cdot 2H_2O$ ). Insoluble (<7%) - Hematite ( $Fe_2O_3$ ), quartz, clay, feldspar.

#### Clean Salt

Appearance: Medium grained (<0.5 cm), white crystalline material. No obvious inclusions of other material.

Composition: Major component of halite, traces of anhydrite ( $CaSO_4$ ), quartz, feldspar.

The sample preparation and measurements were performed as previously described. Two samples of each of the clean and dirty salts were run. The dirty salt exhibited an endotherm between 605 and 645 K which is believed to be associated with polyhalite dehydration. The scan of the clean salt did not show any thermal anomalies. The results are shown in Table III.

Since the inaccuracy of the DSC specific heat determinations is estimated to be no greater than  $\pm 5\%$ , it can be seen that the specific heats of the clean and dirty salts were identical within the limits of experimental error, and both were identical to the specific heat reported for pure NaCl.

Table III

Specific Heat Results for the Clean and Dirty Salt Samples from ERDA#9  
(kJ/kg-K)

Sample No. T(K)	Clean Salt		Dirty Salt		NaCl <sup>3</sup>
	#1	#2	#1	#2	
298	0.85	0.85	0.86	0.86	0.87
400	0.90	0.90	0.90	0.90	0.90
500	0.94	0.93	0.93	0.93	0.93
600	0.96	0.96	0.96	0.96	0.95
700	0.98	0.98	0.98	0.98	0.98

Although the above results indicate that the specific heat of samples composed largely of halite is identical to that of pure NaCl, no measurements were made on samples composed principally of polyhalite or anhydrite, in contrast to the expansion and conductivity measurements. It would be desirable to examine the specific heats of these minerals if future thermal properties studies are conducted.

### III. Thermal Expansion Measurements

The thermal expansion measurements were performed at the Dynatech Corp., Cambridge, MA with a Netzsch automatic recording quartz single pushrod dilatometer. The dilatometer was operated in an ambient environment and in a temperature range 293-700 K. A standard specimen of sapphire ( $\text{Al}_2\text{O}_3$ ) was used to calibrate the dilatometer. The net overall error limit associated with these measurements is estimated to be  $\pm 5\%$ .

The specimens for the dilatometer were saw cut at Dynatech to a rectangular parallelepiped shape with dimensions  $\sim 50 \text{ mm} \times 12 \text{ mm} \times 12 \text{ mm}$ . Since 12 mm is about the same size as a linear dimension of the larger crystallites in the core samples, some breakage of samples along crystallite boundaries occurred during the experiments. Out of a total of 15 samples, three samples broke after being subjected to 400 K and six disintegrated after exposure to 600 K. Two cores (#2, #3) could not be cut to yield a suitably sized sample. The initial length of each sample was measured with a micrometer. The results from the Dynatech report (Appendix A) are shown in Table IV. The mean coefficient of linear thermal expansion  $\alpha$  is defined by the relation,

$$\bar{\alpha} = \frac{1}{L_0} \frac{\Delta L(T_{\text{max}})}{(T_{\text{max}} - 293 \text{ K})},$$

where  $L_0$  = initial length and  $\Delta L(T_{\text{max}})$  is the sample elongation, at  $T_{\text{max}}$ , the highest temperature achieved in Table IV. Also shown in the last row of Table IV are the TPRC recommended expansion values and mean expansion coefficient for NaCl.<sup>4</sup> The data for the samples which survived to 600 C or above is shown graphically in Fig. 1 along with the Thermophysical Properties Research Center (TPRC) recommended expansion curve for NaCl.

From inspection of Table IV and Fig. 1 it is evident that there are two distinct groups of samples with different thermal expansion characteristics. The

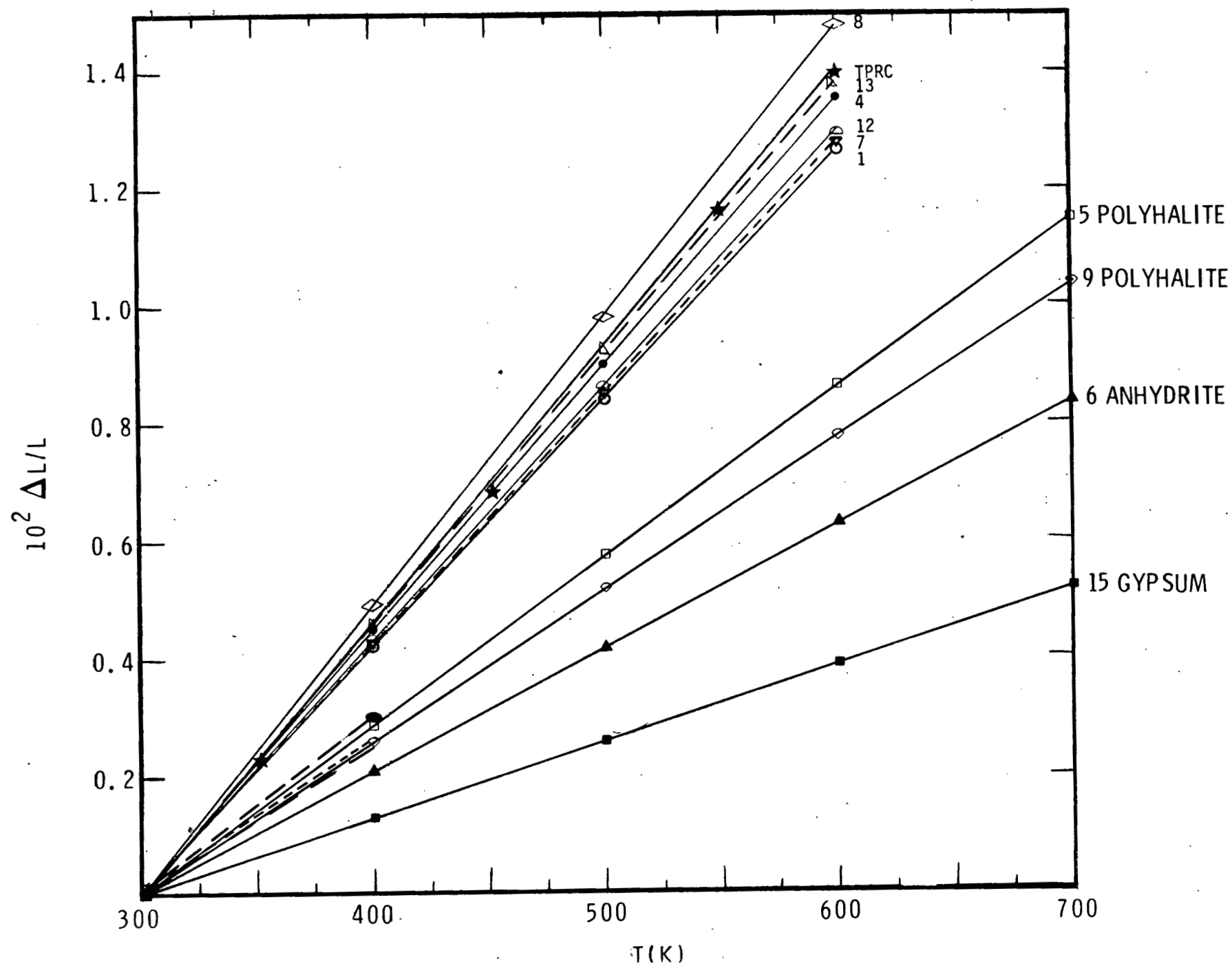


Fig. 1. Thermal expansion vs temperature for samples in Table IV. Also shown is the TPRC recommended expansion for NaCl.



Table IV

## The Linear Thermal Expansion of Salt and Rock Core Specimens - Dynatech

Sample Reference	Temp.	Linear Thermal Expansion, $\Delta L/L_0$						Overall Coefficient Of Linear Thermal Expansion $\alpha(10^{-6}K^{-1})$
		293 K	300 K	( $10^4 \Delta L/L_0$ ) 400 K	500 K	600 K	700 K	
1 2703.5-8 to 2704.7-8		0	2.6	44.3	85.9	127.6	(2)	41.6
2 2055.3-8 to 2056-8		(1)						
3 ERDA 9/2840.7 to 2841.45		(1)						
4 ERDA 9/1908 to 1908.75		0	2.5	46.3	90.2	134.1	(2)	43.7
5 ERDA 9/1910.3 to 1910.9		0	1.3	29.7	58.2	86.6	115.1	28.3
6 ERDA 9/1631.4 to 1632		0	0.4	20.9	41.5	62.0	82.6	20.3
7 ERDA 9/1086.8 to 1087.55		0	1.3	44.0	86.8	129.5	(2)	42.2
8 ERDA 9/1969.4 to 1970.1		0	2.3	49.6	96.8	144.1	(2)	46.9
9 AEC#8MB133/2001.9 to 2002.7		0	1.5	27.2	52.8	78.5	104.2	25.6
10 AEC#8/1995.6 to 1996.1		0	1.8	27.8	(2)	(2)	(2)	26.0
11 AEC#8/698 to 698.5		0	2.0	30.8	(2)	(2)	(2)	28.8
12 AEC#8/1212.25 to 1213.1		0	1.3	44.4	87.6	130.1	(2)	42.4
13 AEC#8/2062.6 to 2063.2		0	2.1	47.2	92.2	137.3	(2)	44.7
14 WIPP#19/616 to 617		0	1.9	27.6	(2)	(2)	(2)	25.8
15 WIPP#19/267.35 to 268.35		0	0.1	12.7	25.6	38.4	51.2	12.6
TPRC-NaCl (recommended)		0	2.8	44.8	89.6	137.1	---	44.7

(1) Samples suitable for measurement could not be obtained from the core material.

(2) Sample decomposed.

first group, comprised of samples from cores #1, 4, 7, 8, 12 and 13, had expansions close to that of pure NaCl. Table I indicates that each of these cores contained sizeable fractions of halite, and the dilatometer samples were in fact cut from the halite portions of these cores. A second group of samples taken from

cores #5, 6, 9, and 15 had much lower expansions, ~0.3-0.5 that of NaCl. Cores #5 and #9 were principally polyhalite, and Fig. 1 shows that they had very similar expansion values. Core #6 was anhydrite and Core #15 siltstone and gypsum.

Although the sample sizes used in this study were too small to be representative of large cores, they did provide some useful information. The expansion of the halite in the core samples appears to be close to that of pure NaCl. The largest deviation from the published NaCl expansion at 600 K was about 8%. The presence of some small cracks or joints in our samples does not appear to have produced a noticeable affect on the thermal expansion behavior. The expansion of the other minerals in the core samples is lower, with anhydrite and polyhalite having about half the expansion of halite. This information can be used to predict the linear expansion of a region in the repository if the composition and mineral arrangement in that region are known.

#### IV. Thermal Conductivity Measurements and Analysis

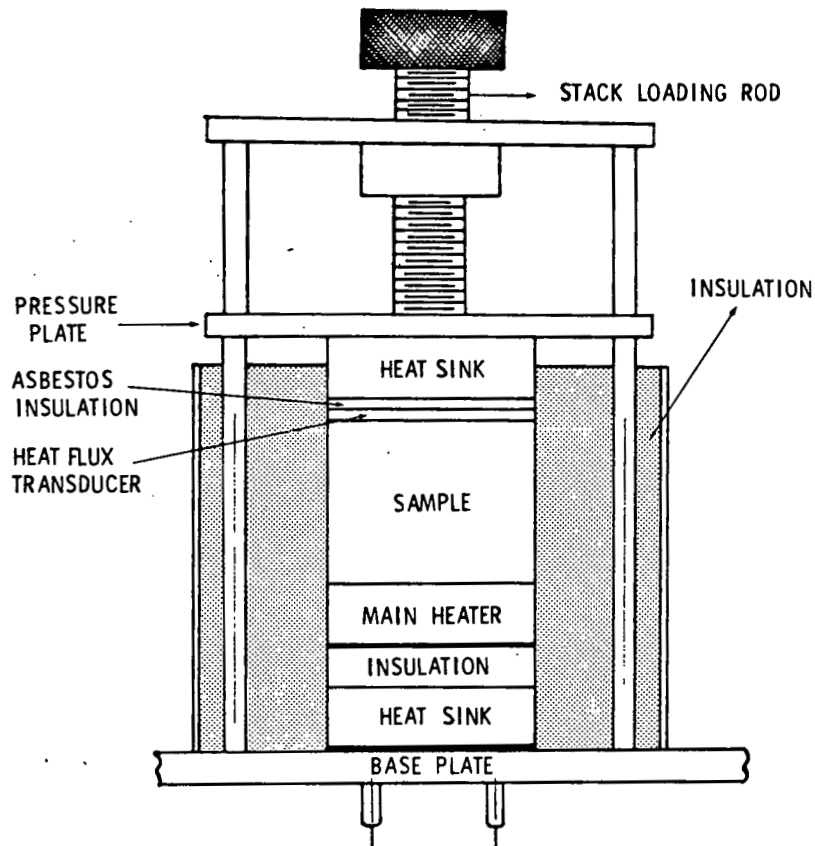
In this section, the thermal conductivity measurements are described and the results analyzed. A preliminary discussion of these topics was given in Ref. 1. In part A, the measurement techniques are described and the measurement results are presented in part B. In part C, the theory of salt thermal conductivity is reviewed and past measurements are discussed, and in part D an analysis of the sensitivity of repository temperatures to thermal conductivity variation is presented. The conclusions of this part of the study are presented in part D.

##### A. Thermal Conductivity Measurement Techniques

The thermal conductivity of the salt specimens used in this study was measured at three different laboratories, each of which used a different technique. At Sandia Laboratories, Albuquerque, NM, the linear heat flow technique described by Acton<sup>5</sup> was used, while at the Los Alamos Scientific Laboratories (LASL), Los Alamos, NM, a transient line source method was employed.<sup>6</sup> Finally, in a recent series of measurements performed at the Dynatech Corp., Cambridge, MA, a linear heat flow thermal comparator technique was utilized.<sup>7</sup>

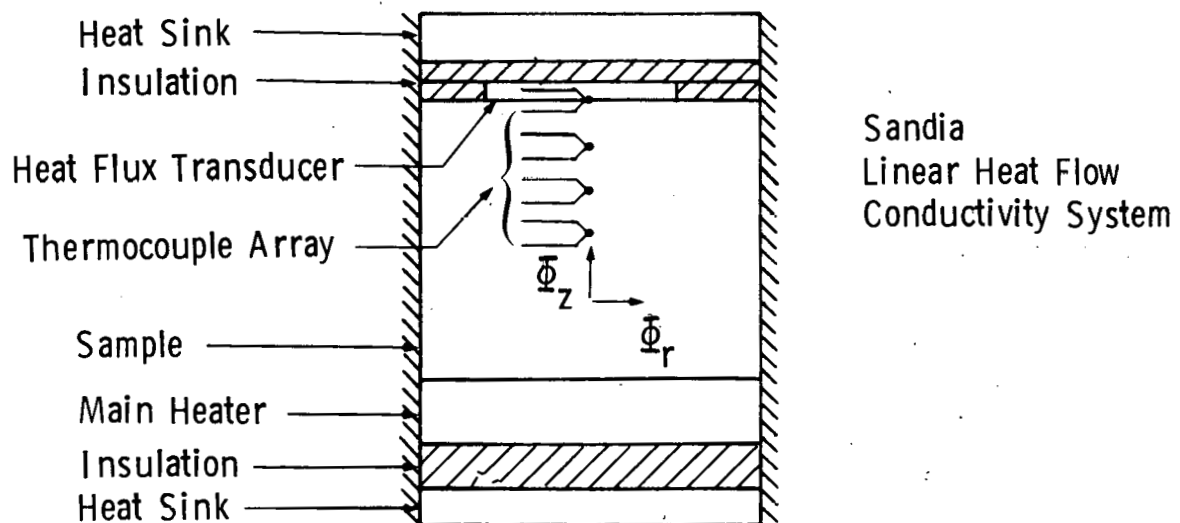
The initial measurements in this program were made at Sandia using the linear heat flow technique, in an extension of Acton's work.<sup>5</sup> The samples were taken from well ERDA#9 at the 630 m and 799 m level. In a later experiment, a sample of pure pressed granulated salt was measured both at Sandia and at Dynatech in order to make a direct comparison of the results obtained by both laboratories on samples obtained for the same piece of homogeneous material.

In the Sandia linear heat flow technique a system of the type shown in Fig. 2(a) is used with a cylindrical sample of nominal dimensions 10 cm high and 10 cm in diameter. Heat is supplied from a bottom or main heater and flows axially up the sample and radially out the sides into a powder insulation. The system does not employ guard heaters. The centerline temperature profile is determined from thermocouples



SLA THERMAL CONDUCTIVITY APPARATUS SCHEMATIC

Fig. 2. (a) Diagram of the Sandia linear heat flow conductivity apparatus. The system is not guarded.



(b) Schematic diagram of the linear flow system.  $\phi_z$  = axial heat flux and  $\phi_r$  = radial or leakage heat flux.

imbedded in radial holes drilled in the sample and the heat flux at the cold or top end is determined with a heat flux transducer, as shown in Fig. 2(b). Further details are given in Ref. 5. The thermal conductivity is determined from the relation,

$$\lambda = \phi_z(L)/(dT/dz)_L \quad , \quad (1)$$

where  $\phi_z(L)$  is the axial heat flux measured by the transducer at  $z = L$  and the derivative  $dT/dz$  is calculated from a least squares polynomial fit to the  $T(z_i)$  data, where the  $z_i$  are thermocouple axial locations. The advantage of this technique is that it uses a large sample which is relatively easy to machine and install in the heater apparatus. The principal disadvantage is that it is most sensitive to the conductivity at the cold end ( $z = L$ ) and fairly insensitive to the conductivity at the other end. Hence, it will not provide an average conductivity of inhomogeneous samples but rather a conductivity which is heavily weighted by the conductivity in the region of  $z = L$ . Another disadvantage of the method is that it relies on the heat flux transducer calibration data supplied by the manufacturer for determination of the heat flux from the measured transducer output voltage and temperature.

In the sample preparation process, core samples from the ERDA#9 drill hole were machined to produce cylindrical samples 108 mm in diameter and 102 mm high. Six equally spaced 1.6 mm diameter thermocouple holes were drilled radially to the central axis of the sample. The holes were located symmetrically with respect to the  $z$  axis midpoint. The sample rested on the main heater which consisted of a nichrome wire wound heater sandwiched between zirconia tiles. A Pb foil was located between the top of the sample and the heat flux transducer to improve contact between the sample and transducer. The transducer was a Thermonetics Corp. model no. H11-45-3-E with a square active area 50.8 mm on a side. The manufacturer's reported accuracy is 3%, with the heat flux being determined from the

transducer output voltage via a calibration curve supplied by the manufacturer. The transducer functions by using a thermopile to convert the temperature drop produced by the incident heat flux to an output voltage. Asbestos paper strips were placed between the flux transducer and the upper heat sink to protect the transducer. A screw drive was utilized to bring the heat sink in contact with the stack and to apply stack pressure. Powdered silica insulation was used around the stack to reduce radial heat losses.

In the measurement process, a constant power was supplied to the main heater and a 24 h period was allowed for all sample temperatures to stabilize. The thermocouple and transducer readings were then recorded and the conductivity calculated from Eq. (1). The quantity  $(dT/dz)_{z=L}$  was calculated from a second order least squares polynomial fit to the  $T(z_i)$  data, where the  $z_i$  are the thermocouple axial coordinates. The presence of a significant radial heat flux results in a decrease in  $\phi_z$  as  $z \rightarrow L$ , with the result that  $dT/dz$  decreases as  $z \rightarrow L$ . In practice, a second order polynomial was sufficient to accurately reproduce the  $T(z_i)$  data for all samples measured.

The transient line source or probe method used at LASL is illustrated schematically in Fig. 3. A cylindrical sample is used with a heater probe installed in an axial hole drilled along the sample centerline. A temperature sensor attached to the probe measures the temperature near the probe surface. The sample is surrounded with insulating powder and heated to a nearly uniform temperature with an external cylindrical heater. At the time  $t = 0$  the heater probe is energized with a dc power supply, producing a constant radial heat flux characterized by a linear power density  $\Phi$ (W/m) along the probe. For times  $t$  satisfying  $t > a^2/4\alpha$ , where  $a$  = probe radius and  $\alpha$  = thermal diffusivity of sample, the temperature is given approximately by,<sup>8</sup>

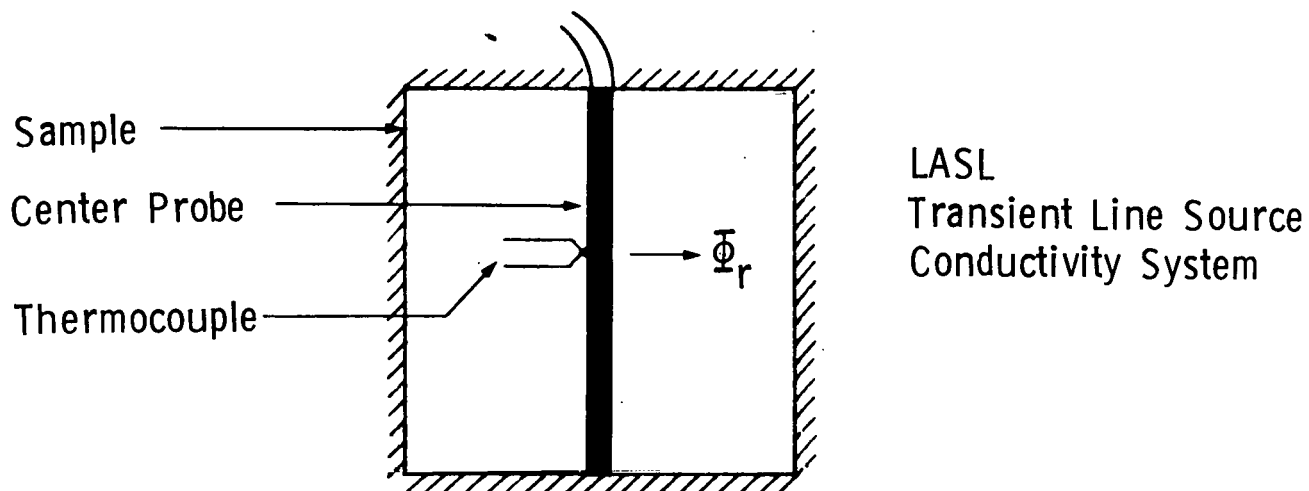


Fig. 3. Schematic diagram of the transient line source system used for thermal conductivity measurement at the Los Alamos Scientific Laboratory.

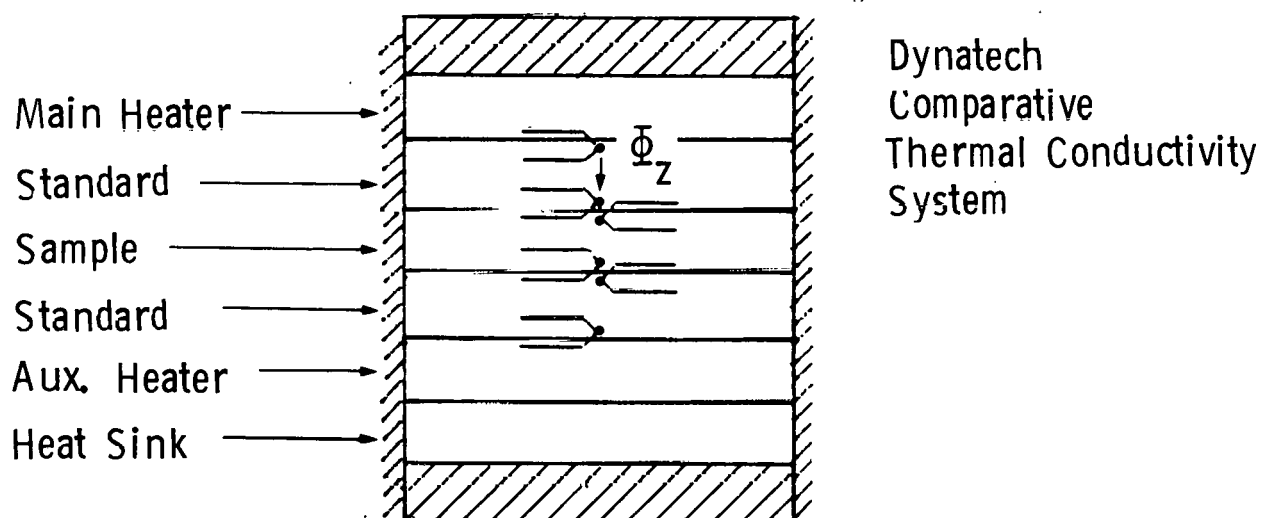


Fig. 4. Schematic diagram of the comparative thermal conductivity system used at the Dynatech Corp.



$$T(a,t) = \frac{\Phi}{4\pi\lambda} [\ln(4\alpha t/a^2) - y] \quad , \quad (2)$$

where  $y$  is Euler's constant. A plot of  $T(a,t)$  vs  $\ln t$  thus has a slope  $\Phi/4\pi\lambda$  from which  $\lambda$  may be derived. Although this technique appears to be absolute since the determination of  $\Phi$  is from highly accurate measurements of the probe voltage and current, in reality end effect losses and probe-sample contact resistance make the calculation of  $\Phi$  somewhat indeterminate. As a result of this, the system is usually calibrated with a quartz specimen of known conductivity.

In the LASL experiments, four samples were cut from two different cores taken from the 631 m and 700 m levels of ERDA#9. The samples were cylindrical with a diameter = 635 mm and height = 365 mm. A 1 mm diameter hole was drilled axially through the center of the sample. A stainless steel probe containing a heater and a thermistor was inserted into the hole and a conductive graphite-glycerin solution was poured into the hole around the probe in order to minimize the thermal contact resistance. The sample was brought to thermal equilibrium at the desired ambient temperature by circulating fluid from a control bath through a coil system wound around the copper sample container. At the time  $t = 0$  a constant electrical input power is supplied to the probe heater of a magnitude sufficient to produce a 4-5 C temperature rise with a few seconds. After a 20 s time delay, thermistor readings were taken every 10 s. The conductivity was then found from Eq. (2) as described above.

The comparative technique employed by Dynatech is illustrated in Fig. 4. A cylindrical sample of height 127 mm and diameter in the range 50-60 mm with thermocouple grooves machined on the top and bottom surfaces is sandwiched between two reference or standard disks of similar size and known conductivity with thermocouples placed in grooves along the top and bottom surfaces of each reference disk. The stack composed of sample and reference disks is sandwiched between a main and auxiliary heater and

the total stack is loaded hydraulically to reduce thermal contact resistance between various stack elements. Three cylindrical guard heaters are used to minimize radial heat transport from the stack. The heat flux  $\phi_z$  through the sample is calculated as the average of the heat fluxes through the top and bottom references,

$$\phi_z = \frac{1}{2} [\lambda_{r1} \Delta T_{r1} / z_{r1} + \lambda_{r2} \Delta T_{r2} / z_{r2}] \quad , \quad (3)$$

where  $\lambda_{r1,2}$  = conductivity of the top (1) and bottom (2) references,  $\Delta T_{r1,2}$  is the temperature drop across the reference and  $z_{r1,2}$  is the reference thickness. The sample conductivity is then given by

$$\lambda_s = \phi_z / (\Delta T_s / z_s) \quad , \quad (4)$$

where  $\Delta T_s$  and  $z_s$  are the temperature drop across the sample and sample thickness respectively. The reference materials used in this investigation were Pyrex 7740 for conductivities in the range ~0.5-1.8 W/m-K and Pyroceram 9606 for conductivities in the range ~2.5-6 W/m-K. The conductivities of the reference materials were assumed to be those published by the National Bureau of Standards for these materials (see Appendix B).

For the comparative measurements, core samples from AEC#8, ERDA#9, and WIPP#19 drill holes were shipped to Dyantech Corp., Cambridge, MA. The cores were machined there to produce disk-shaped samples either 51 mm or 64 mm in diameter by 12 mm in height. Thermocouple grooves were then machined in both faces of the sample and the thermocouples were placed with the junction at the sample axial centerline. These thermocouples were held in place with Astroceram adhesive. The test stack shown schematically in Fig. 4 was then assembled and loaded hydraulically to reduce contact resistance. The stack was surrounded by a coaxial three element guard furnace in order to minimize radial heat flux in the

top and bottom reference and sample elements. The top and bottom guard heaters were controlled by temperature sensors to match the temperatures of the main and auxiliary heater thermocouples respectively, while the central guard heater temperature was matched to the sample average temperature. In this way, the axial temperature distribution at the guard radius was maintained close to that existing at the stack centerline, thus minimizing radial gradients. Dynatech experiments have shown that this type of guarding together with a sample with a diameter/height ratio  $\geq 3$  will result in a fairly uniform axial heat flux throughout the stack; i.e.,  $\phi_z(r,z) \approx \text{constant}$  in the stack.

Measurement errors in the comparative technique are believed to occur principally from two sources, thermal contact resistance between the reference disks and the sample disk and thermal conductivity mismatch between reference and sample which produces a nonlinear  $T(z)$  variation at the stack centerline.<sup>8</sup> The analysis by Laubitz in Ref. 8 indicates that the presence of contact resistance will result in an overestimate of the true sample conductivity. The effect of sample-reference conductivity mismatch is more complex, but generally, for  $\lambda_r > \lambda_s$ ,  $\lambda_s$  is underestimated and for  $\lambda_r < \lambda_s$ ,  $\lambda_s$  is overestimated. In order to make a quantitative estimate of these errors, a numerical heat transfer analysis of the comparator system would be required.

In the Dynatech instrument calibration and verification program (Appendix B), a Pyroceram 9606 reference disk was used as a sample and run against Pyrex 7740 references. The actual data is shown in Appendix B, p. 12. Measurements were made at five temperatures in the range 309-712 K, with the largest observed difference between the measurements and the NBS values being 6% at 309 K. This calibration suggests that the instrument errors are probably not large. In the

absence of any other way to calibrate the system, we have estimated the error associated with the comparative measurements as  $\pm 6\%$  of the measured value.

#### B. Thermal Conductivity Measurement Results

The results of the Dynatech and Sandia experiments are shown in Fig. 5. The top curves show results of Sandia measurements on two samples from ERDA#9. The hysteresis effect seen in the ERDA#9 630 m measurement is believed to be due to water driveoff during the heating process. The numbers on the other curves in Fig. 5 correspond to the same numbers in the first column of Table I. The majority of the samples measured had 300 K conductivities in the range  $\sim 4.5$ – $5.5$  W/m-K. For the samples with  $\lambda(300\text{ K}) < 4.5$  W/m-K (numbers 5, 9, 11, 12, 14), Table I shows that each had a substantial amount of nonsalt material, either polyhalite, clay, or gypsum. The lowest conductivity measured (#14) was from a near surface sample taken from WIPP#19 at the 188 m level. It was composed entirely of laminated gypsum.

The LASL results are shown in Fig. 6 for samples from the 631 m and 799 m levels of ERDA#9. These measurements were made up to only 335 K, the upper limit of the LASL conductivity apparatus. Two samples 6.4 cm in diameter and 3.7 cm high were cut from each of the  $\sim 10$  cm diameter x 20 cm high drilled blocks from each well. It can be seen that the conductivity of all of the samples exhibited about the same temperature dependence but that the magnitude of the conductivity of the two samples from the 631 m ERDA#9 core block differed by about 15%. This is quite typical of the variation which can be found in samples from nearby regions and it occurs because of local inhomogenities in the geologic material. Also shown in Fig. 6 is a line characterized by the relation,  $\lambda = 5(300/T)^{1.14}$  W/m-K, which represents a reasonably good fit to the Dynatech data, as will be discussed in part IV-C.

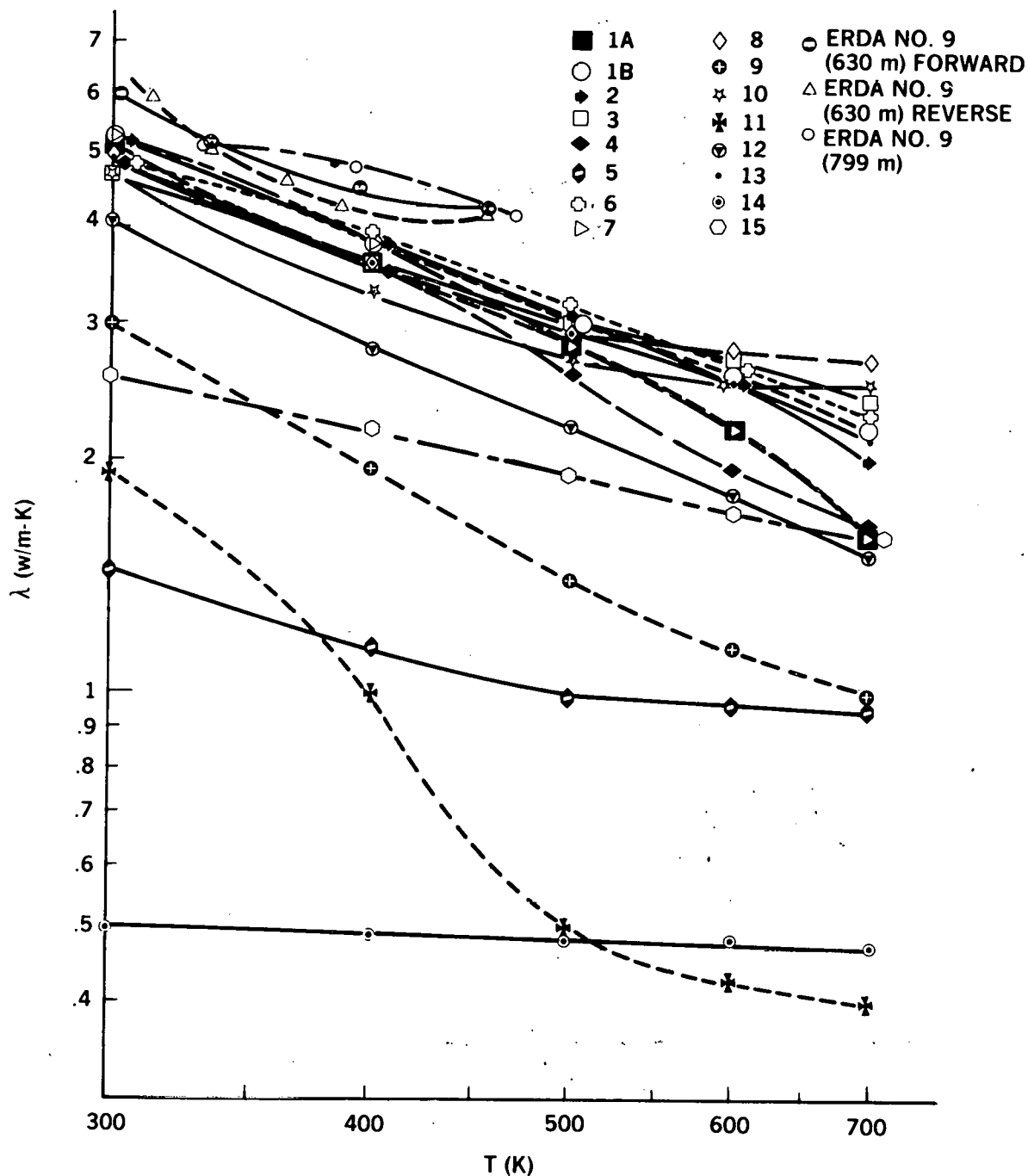


Fig. 5. Experimental conductivity vs temperature results from Dynatech (samples 1A-15) and Sandia (ERDA#9 forward (temp. increasing) and reverse (temp. decreasing) - 630 m and ERDA#9 - 799 m). The sample numbers correspond to the numbers in the first column of Table I.

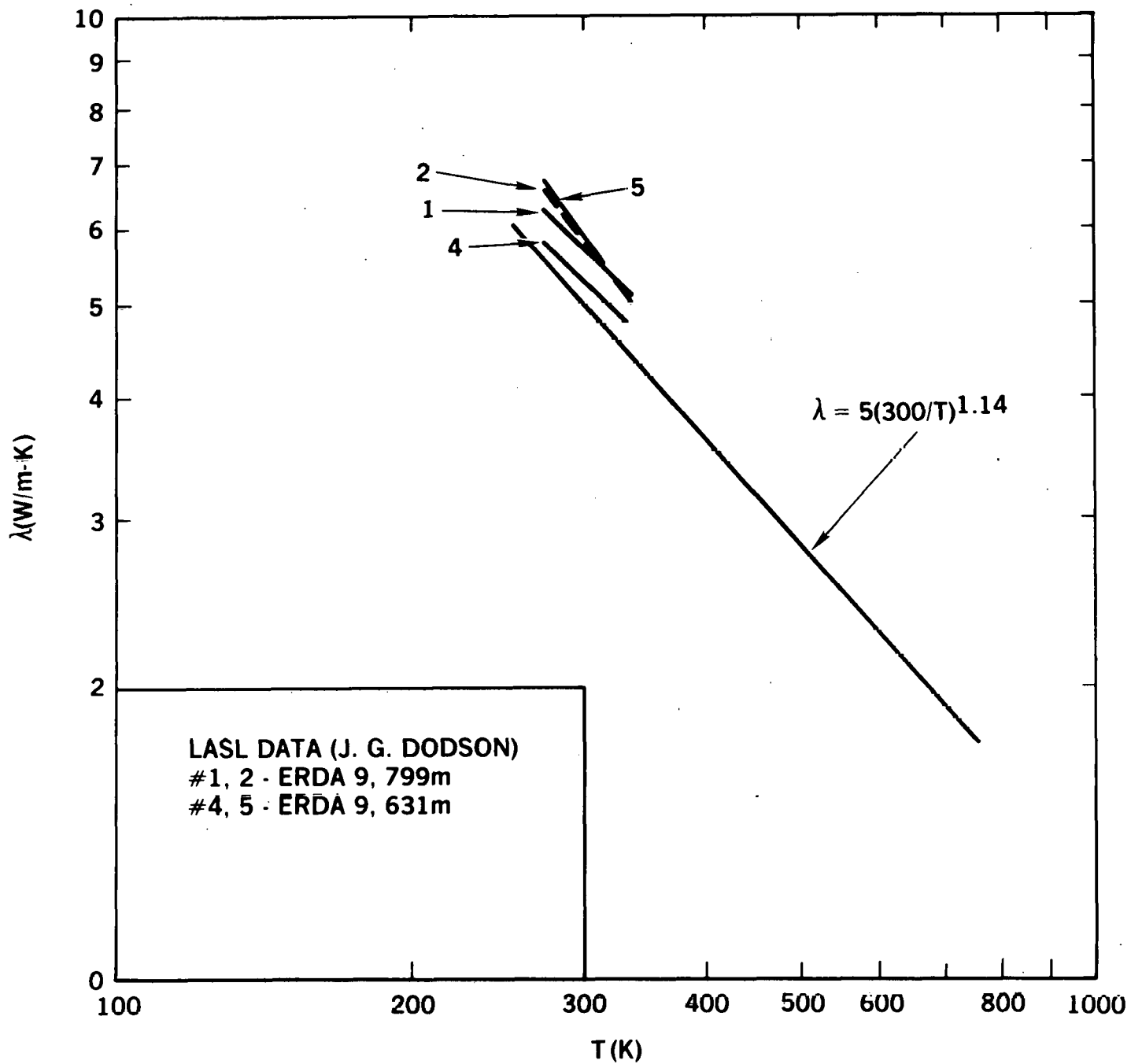


Fig. 6. Experimental conductivity results obtained by LASL for four different samples from two different depths of well ERDA#9. Also shown is the relation,  $\lambda = 5 (300/T)^{1.14}$  which characterizes the Dynatech data.

For comparison purposes conductivity measurements on samples of pure granulated salt cut from a salt block furnished by the Morton Salt Co. were made at both Dynatech and Sandia. The results are shown in Fig. 7, where the Dynatech results are shown (solid line • data points) compared to the Sandia results (dashed lines) for two different runs in which different heat flux transducers were employed. Also shown are the rocksalt conductivity results of Birch and Clark<sup>9</sup> which have been used extensively in the past for thermal modeling of salt repositories, and a curve (dot-dash) represented by the relation,

$$\lambda = \lambda_0 (300/T)^\gamma, \quad (5)$$

where  $\lambda_0 = 5$  W/m-K and  $\gamma = 1.14$ . Eq. (5) represents a fit, accurate to  $\approx \pm 5\%$ , to most of the Dynatech data shown in Fig. 5 for samples composed primarily of halite and anhydrite. The Birch and Clark data can also be characterized by Eq. (5), but with  $\lambda_0 = 5.5$  W/m-K and  $\gamma = 1.20$ . The effect of variation in heat flux transducers or uncertainty in their calibration in the Sandia experiments is indicated by the shift in the Sandia data by about 25% produced by the transducer exchange. The estimated  $\pm 6\%$  maximum error for the Dynatech data is represented by the error bar at the 320 K point on the Dynatech  $\lambda$  vs T graph in Fig. 7.

In the case of the Sandia data, it is evident that the conductivity difference observed with the two different flux transducers was much larger than the quoted  $\pm 3\%$  accuracy of the transducers. In addition, the observed temperature dependence of the Sandia  $\lambda$  vs T curves in Fig. 7 is not the same as that observed in the Dynatech experiments or that reported by Birch and Clark. There is, however only a  $\sim 30\%$  discrepancy between the SLA and the Dynatech results. In view of the better calibration of the Dynatech experimental equipment and the substantial agreement between the Dynatech results and those of Birch and Clark over a large temperature range, we have elected to use the Dynatech data as the primary results



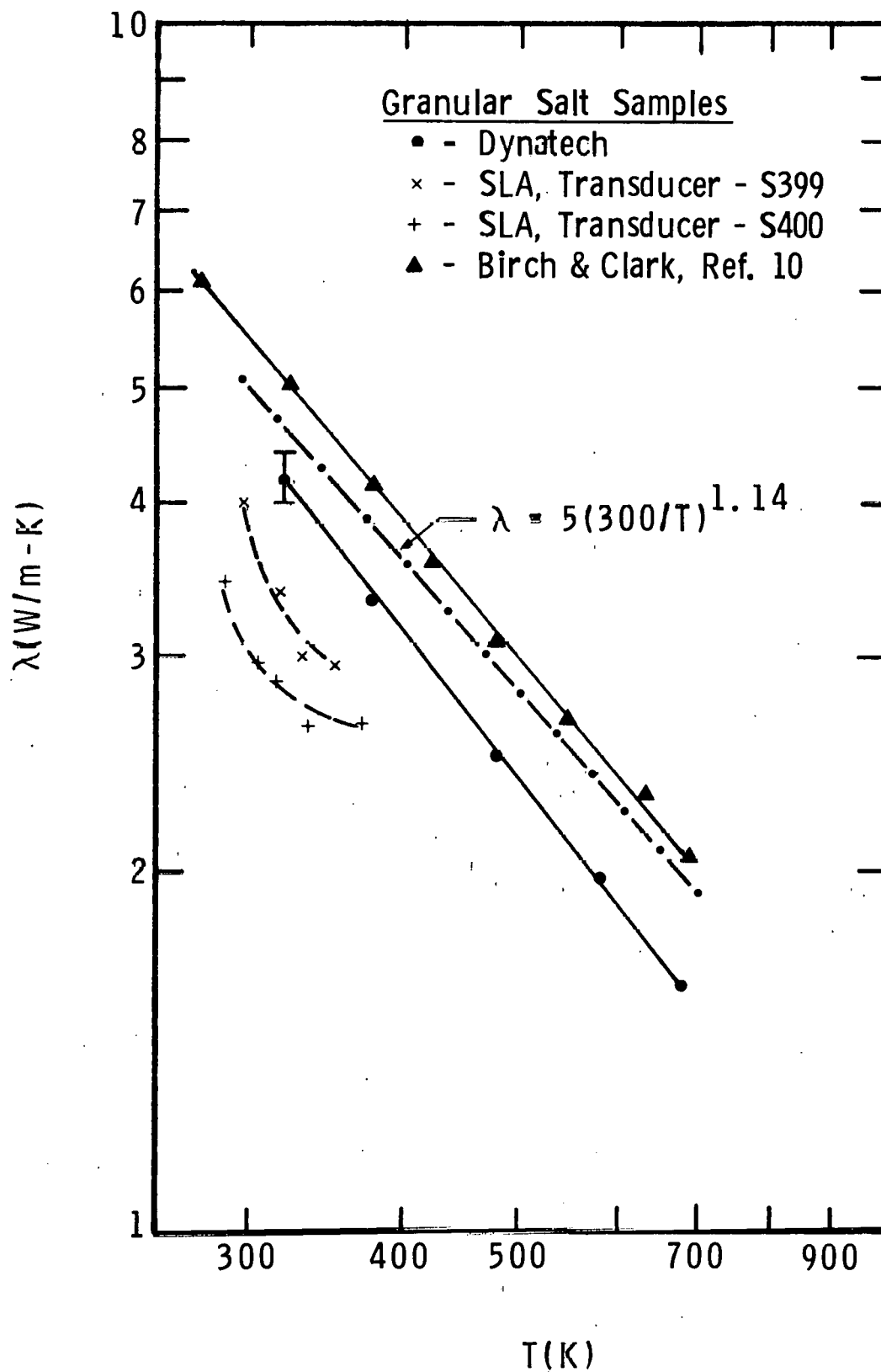


Fig. 7. Comparison of Dynatech and Sandia data for similar samples of 99% pure granulated salt cut from a salt block furnished by the Morton Salt Co. Also shown is the data of Birch and Clark (Ref. 9) and the function given by Eq. (5) which fits the Dynatech data for WIPP rocksalt.

of this investigation. The Sandia results confirm the general magnitude and trend of the conductivity data, but they cannot be relied upon as a primary data source. In the following section we shall discuss the theory of insulator conductivity and show that Eq. (5) rests on a reasonably sound theoretical foundation.

### C. Theory of Salt Thermal Conductivity and Review of Past Measurements

1. Review of Thermal Conductivity Theory. The basic theory of insulator thermal conductivity is reasonably well established, although the complexity of this theory makes it difficult to achieve close numerical correspondence between theory and experiment without use of adjustable parameters or simplifying approximations. In the case of opaque insulators, heat is transported by acoustic phonons, and scattering of these phonons, either by other phonons or by imperfections such as dislocations or grain boundaries, produces a resistance to heat transport. The theory of lattice thermal conductivity has been reviewed extensively by Klemens<sup>10,11</sup> and Ziman,<sup>12</sup> and an extensive list of references has recently been compiled by Slack.<sup>13</sup> The purpose of this review is to discuss those aspects of the theory which pertain to the conductivity of rocksalt and to discuss the temperature dependence of this conductivity.

In a material such as rocksalt with reasonably large sized crystals, boundary and imperfection scattering is relatively unimportant, with the result that the main source of thermal resistance is phonon-phonon scattering. The most important events are three phonon processes which have their basis in the anharmonic terms in the Hamiltonian which describes the oscillating crystal lattice.<sup>12</sup> The lowest order anharmonic term contains all possible products of three atomic displacements. When this term in the Hamiltonian is transformed to its quantized form, it describes three phonon processes in which either one phonon is destroyed with two being created or the inverse process with two phonons interacting to form

a third. In these interactions, energy is conserved and crystal momentum is conserved up to a reciprocal lattice vector. In the case of an interaction in which two phonons with wave vectors  $\vec{k}'$  and  $\vec{k}''$  are destroyed with the creation of a phonon with wave vector  $\vec{k}$ , a process with,

$$\vec{k}' + \vec{k}'' = \vec{k} \quad (6)$$

is called a normal or N process, while a process with

$$\vec{k}' + \vec{k}'' = \vec{k} + \vec{G} \quad , \quad (7)$$

where  $\vec{G}$  = reciprocal lattice vector is called an "umklapp" or U process. If there is a nonequilibrium phonon distribution produced by a temperature gradient, N processes alone cannot restore equilibrium when the gradient is removed because N processes leave the total phonon momentum unchanged, as indicated by Eq. (6). Thus U processes are required for restoration of thermal equilibrium, even though the value of the thermal conductivity depends on both types of processes.

At temperatures  $\gtrsim \theta_D$ , the Debye temperature, all phonon modes are excited and the conductivity is determined principally by U processes. For NaCl,  $\theta_D$  is in the range  $\sim 250$ - $300$  K, with the exact value dependent on the way in which  $\theta_D$  is derived from experimental data. Thus, in situations of interest for waste repository analysis, the medium will be above  $\theta_D$  and hence in the U process region. For this temperature region, there have been several transport theory calculations of the thermal conductivity performed in an attempt to derive the conductivity magnitude in terms of more fundamental constants and parameters. Leibfreid and Schlömann made the first definitive calculation in 1954.<sup>14</sup> Since that time, their calculation has been corrected and refined by a number of authors as discussed by Parrott and Stuckes.<sup>15</sup> The resulting high temperature phonon conductivity for  $T \gg \theta_D$  as quoted by Parrott and Stukes is,

$$\lambda_{PS} = \frac{24}{5} 4^{1/3} \left( \frac{k_B}{h} \right)^3 \frac{\bar{M} \delta \theta_D^2}{(\gamma + 1/2)^2} \left( \frac{\theta_D}{T} \right), \quad (8)$$

where  $k_B$  = Boltzmann's constant,  $h$  = Planck's constant,  $\bar{M}$  = mean atomic mass,  $\delta$  = cube root of mean atomic volume, and  $\gamma$  = Grüneisen parameter. In the Debye model,  $\gamma$  is defined via the relation,  $\gamma = -\partial(\ln \theta_D) / \partial(\ln V)$ , where  $V$  = crystal volume. Slack has proposed a slightly modified version of Eq. (3) as being more consistent with experimental data for a range of different materials. The Slack conductivity is given by the relation,<sup>16</sup>

$$\lambda_S = B n^{1/3} \bar{M} \delta \frac{\theta_D^2}{\gamma^2} \left( \frac{\theta_D}{T} \right)^{1+n_{ex}}, \quad (9)$$

where  $n$  = number of atoms in the lattice basis,  $B = 3.04 \times 10^{-6}$ ,  $\bar{M}$  = mean atomic mass (grams),  $\delta$  = cube root of the mean atomic volume ( $\text{\AA}$ ), and  $n_{ex}$  is a small positive number which arises as a result of both thermal expansion and acoustic-optic phonon interactions.<sup>17</sup>  $\lambda_S$  is in units of W/m-K.

Both Eq. (8) and Eq. (9) yield reasonable values for  $\lambda$  of NaCl.  $\theta_D$  is not uniquely defined, but its value falls in the range  $\sim 250$ - $330$  K, depending on how it is extracted from experimental data. Using the parameters shown in Table VI, the Debye temperature conductivities  $\lambda_{PS}(\theta_D) = 13.88$  W/m-K and  $\lambda_S(\theta_D) = 8.11$  W/m-K are derived.

The TPRC data collection indicates that measured single crystal NaCl conductivities fall in the range,  $\lambda_{exp} \approx 6.5$ - $8.5$  W/m-K at  $T = 250$  K.<sup>20</sup> Thus both Eq. (8) and Eq. (9) predict the magnitude of the salt thermal conductivity reasonably well.

From a simple kinetic theory calculation, it can be shown that the conductivity is related to the U process mean free path  $\ell$  by,

Table VI  
Thermal Parameters for NaCl Used in the Conductivity Calculation

<u>Parameter</u>	<u>Value</u>	<u>Notes/(ref.)</u>
$\theta_D$	250 K	Assumed
$\bar{M}$	29.22 g	Mean of Na and Cl atomic masses.
$\delta$	1.77 Å	FCC crystal, lattice parameter, $a_0$ = 5.63 Å, 8 atoms/FCC cell. (18)
$\gamma$	1.56	High temp. limit (19)
$n$	2	2 atoms/unit cell

$$\lambda = \frac{1}{3} C_v v_s \ell \quad , \quad (10)$$

where  $C_v$  = specific heat (unit volume) and  $v_s$  = a representative sound velocity. Using the representative values  $C_v = 1.88 \text{ J/cm}^3\text{-K}$ ,  $v_s = 5 \times 10^5 \text{ cm/s}$ , and  $\lambda = 7 \text{ W/m-K}$ ,<sup>21</sup> the mean free path is found to be,  $\ell_{\text{NaCl}} = 23 \text{ Å}$ . Thus, the thermal conductivity should not be much affected by the polycrystalline nature of actual dense rocksalt samples until the average grain size decreases to a very small value. The salt data discussed in Sec. IV-B generally supports this hypothesis. In many cases, fairly dirty salt specimens had room temperature conductivities in the range 5-6 W/m-K, and in a large number of other cases,  $\lambda$  (290 K) fell in the range 4-5 W/m-K.

The temperature dependence of  $\lambda$  is important for predicting repository temperature distributions from heat transfer calculations. The classical theory discussed by Parrott and Stuckes predicts  $\lambda \propto T^{-1}$  when  $T \gg \theta_D$ , as indicated by Eq. (8). The theory proposed by Slack leads to the prediction  $\lambda \propto T^{-(1+n_{\text{ex}})}$ , where  $n_{\text{ex}} \sim 0.1$ . For NaCl, Slack has found  $n_{\text{ex}} \approx 0.24$ . The TPRC data indicates that  $n_{\text{ex}} \approx 0.16$ . Klemens<sup>22</sup> has suggested that, for  $T \gtrsim \theta_D$ , the correct form for the temperature dependence of  $\lambda$  is

$$\lambda_K \propto (T - \alpha\theta_D)^{-1}, \quad (11)$$

where  $\alpha \approx 1/3$ . No derivation is presented for this form, but it is suggested that Eq. (11) would result from expanding the phonon distribution functions in the general conductivity expression to second order in  $T^{-1}$  rather than first order, as is commonly done to derive high temperature expressions like Eq. (8). However, an actual expansion of the general expression leads to the cancellation of second order terms as a result of energy conservation in three phonon U processes. As a result of this, we feel that Eq. (11) must be regarded as strictly a phenomenological relation. An equation of this type with  $\alpha\theta_D = 100$  K was used by Stephens and Maimoni<sup>23</sup> to analyze rocksalt conductivity data and also by Acton<sup>5</sup> in a preliminary analysis of New Mexico rocksalt data. The logarithmic temperature derivatives of the various conductivity expressions are shown in Table VII.

Table VII  
Temperature Dependence of Conductivity Expressions for Various Models  
Discussed in the Text

Conductivity Expression	$d(\ln\lambda)/d(\ln T)$	$d(\ln\lambda)/d(\ln T) _{T = \theta_D}$
$\lambda_{PS} \propto T^{-1}$	-1	-1
$\lambda_S \propto T^{-1.24}$	-1.24	-1.24
$\lambda_K \propto (T - \theta_D/3)^{-1}$	$-1/(1 - \theta_D/3T)$	-1.5

In addition to classical phonon heat conduction, heat can also be transferred in semitransparent solids, such as rocksalt, by radiation. In situations where radiant transfer from the boundaries can be ignored in calculating the heat flux within a semitransparent solid, it can be shown that radiant transfer produces a heat flux proportional to the local temperature gradient,<sup>24</sup> with the constant of proportionality or effective radiation conductivity being given by,

$$\lambda_R = \frac{16}{3} \frac{n^2 T^3 \sigma}{\kappa_R} \quad (12)$$

In Eq. (12)  $n$  = mean index of refraction,  $\sigma$  = Stefan-Boltzmann constant, and  $\kappa_R$  is a mean absorption coefficient defined by Viskanta and Anderson.<sup>25</sup>  $\lambda_R$  in Eq. (12) is frequently referred to as the Rosseland radiative conductivity after S. Rosseland who proposed the expression in 1931.

Using Eq. (12), it is possible to estimate values of  $\kappa_R$  which will lead to an appreciable value of  $\lambda_R$ . The Wien displacement law relating the temperature and the wavelength  $\ell_m$  corresponding to the maximum in the blackbody power spectrum is,<sup>26</sup>

$$\ell_m T = 2989 \text{ } \mu\text{m} - \text{K} \quad , \quad (13)$$

when  $\ell_m$  is in  $\mu\text{m}$  and  $T$  in K. At 600 K,  $\ell_m \approx 5 \text{ } \mu\text{m}$ . Using the estimate  $n = 1.5$  in Eq. (12) leads to the result,

$$\lambda_R(600\text{K}) = \frac{1.47 \times 10^2}{\kappa_R} \text{ W/m-K} \quad (14)$$

For  $\lambda_R$  to be non-negligible, say  $\lambda_R \geq 0.5 \text{ W/m-K}$ , requires,

$$\kappa_R \lesssim 300 \text{ m}^{-1} \quad . \quad (15)$$

The limiting value of  $\kappa_R$  in Eq. (15) corresponds to a material with an optical thickness,  $d_R \sim 5/\kappa_R \sim 1.7 \text{ cm}$ . Bulmer has recently completed measurements on the infrared transmittance properties of rocksalt samples obtained from the proposed WIPP site. Measurements were made in the wavelength range  $\sim 3.5\text{-}12.5 \text{ } \mu\text{m}$ .<sup>27</sup> The frequency averaged extinction coefficient which includes both absorption and scattering is reported by Bulmer to fall in the range  $\sim 500\text{-}1000 \text{ m}^{-1}$  for 6.3 mm thick samples and  $\sim 330\text{-}550 \text{ m}^{-1}$  for 12.7 mm thick samples. Essentially zero



transmission was observed for 51 mm thick samples. If all the optical attenuation in the Bulmer experiments was produced by absorption, then Eq. (14) predicts a negligible radiative conductivity at 600 K. If some of the attenuation is due to scattering, then it is not possible a-priori to rule out a radiative contribution to the conductivity at the level of  $\lambda_R \lesssim 0.5 \mu\text{m}$ .

## 2. Review of Past Measurements

A large amount of data on the thermal conductivity of relatively pure rock-salt samples is reported in the TPRC data series.<sup>20</sup> Some of this data which is presented in graphical form is reproduced in Fig. 8. The reported measurements do not extend to a high enough temperature to exhibit radiative conductivity effects; i.e.,  $\lambda \propto T^3$ . In the range  $T \gtrsim 200$  K, the trend of the data follows an expression of the Slack form, Eq. (5), with  $\gamma = 1.16$  and a 300 K conductivity  $\lambda_0 = 6$  W/m-K. The thermal conductivity used by Cheverton and Turner<sup>28</sup> in an analysis of the proposed Lyons, Kansas waste repository was of the form given by Eq. (5) with  $\lambda_0 = 5.5$  W/m-K and  $\gamma = 1.21$ . They obtained their data from Birch and Clark.<sup>9</sup> In a recent analysis of temperatures in a bedded salt repository produced by high level waste canisters, Sisson<sup>29</sup> used a conductivity which, in the range  $T = 325$ -460 K, falls in between the TPRC and the Birch and Clark conductivities and which does not have the form of Eq. (5). The Birch and Clark, Sisson, and TPRC conductivities are shown graphically in Fig. 9. Also shown in Fig. 9 is some Oak Ridge National Laboratory data on single crystal rocksalt from Lyons, Kansas.<sup>30</sup> Data reported by Acton<sup>5</sup> for a rocksalt sample taken from a Mississippi Chemical Co. potash mine in southeast New Mexico is also shown in Fig. 9. This data is characterized by  $\lambda_0 = 8$  W/m-K and  $\gamma = 1.02$ . Acton also measured some rocksalt samples from the site of the proposed Waste Isolation Pilot Plant (WIPP) near Carlsbad, NM. The samples were taken from a well designated AEC-8 and are shown in Fig. 10.

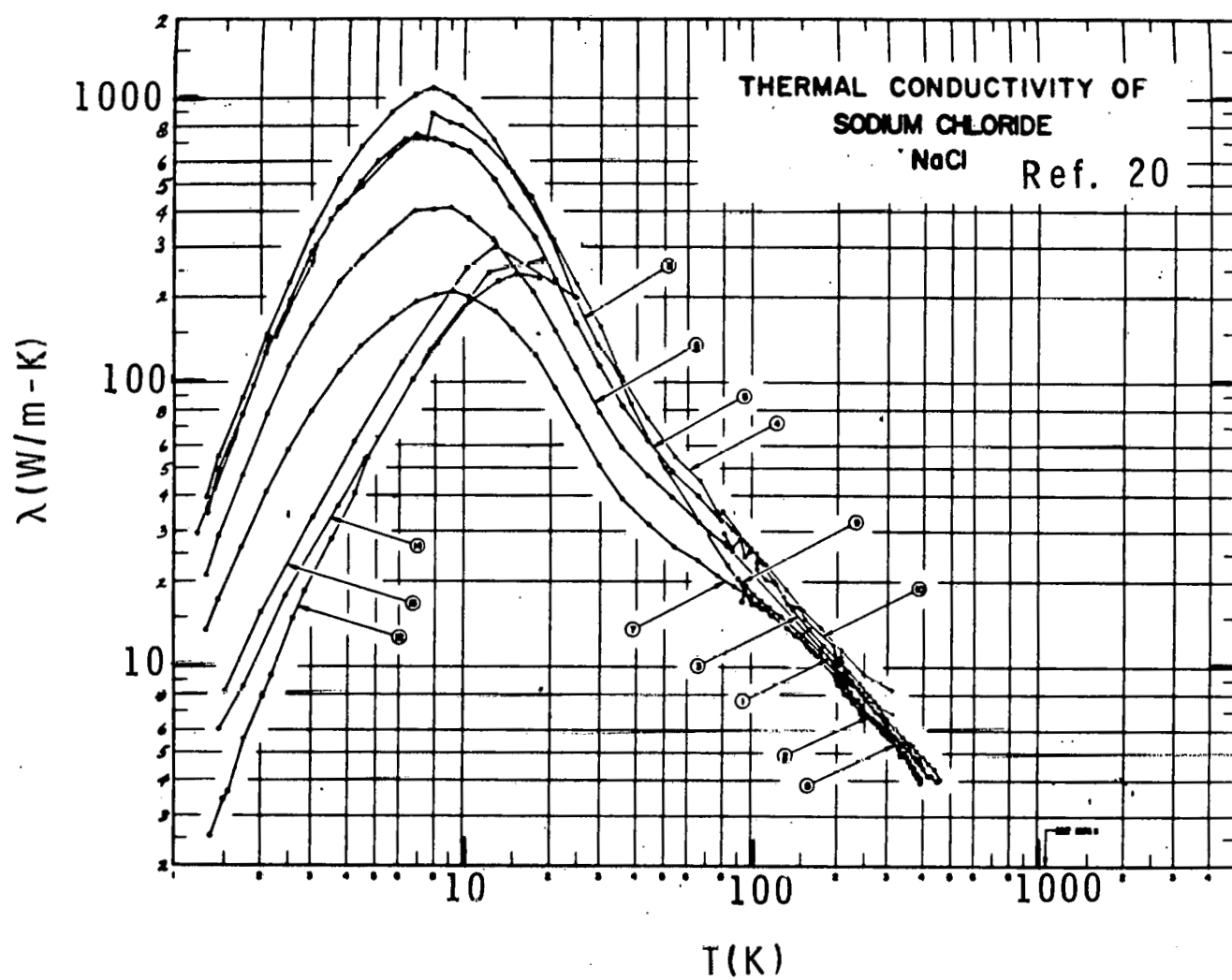


Fig. 8. Thermal conductivity vs temperature of rocksalt as reported in the TPRC Data Series (Ref. 20).

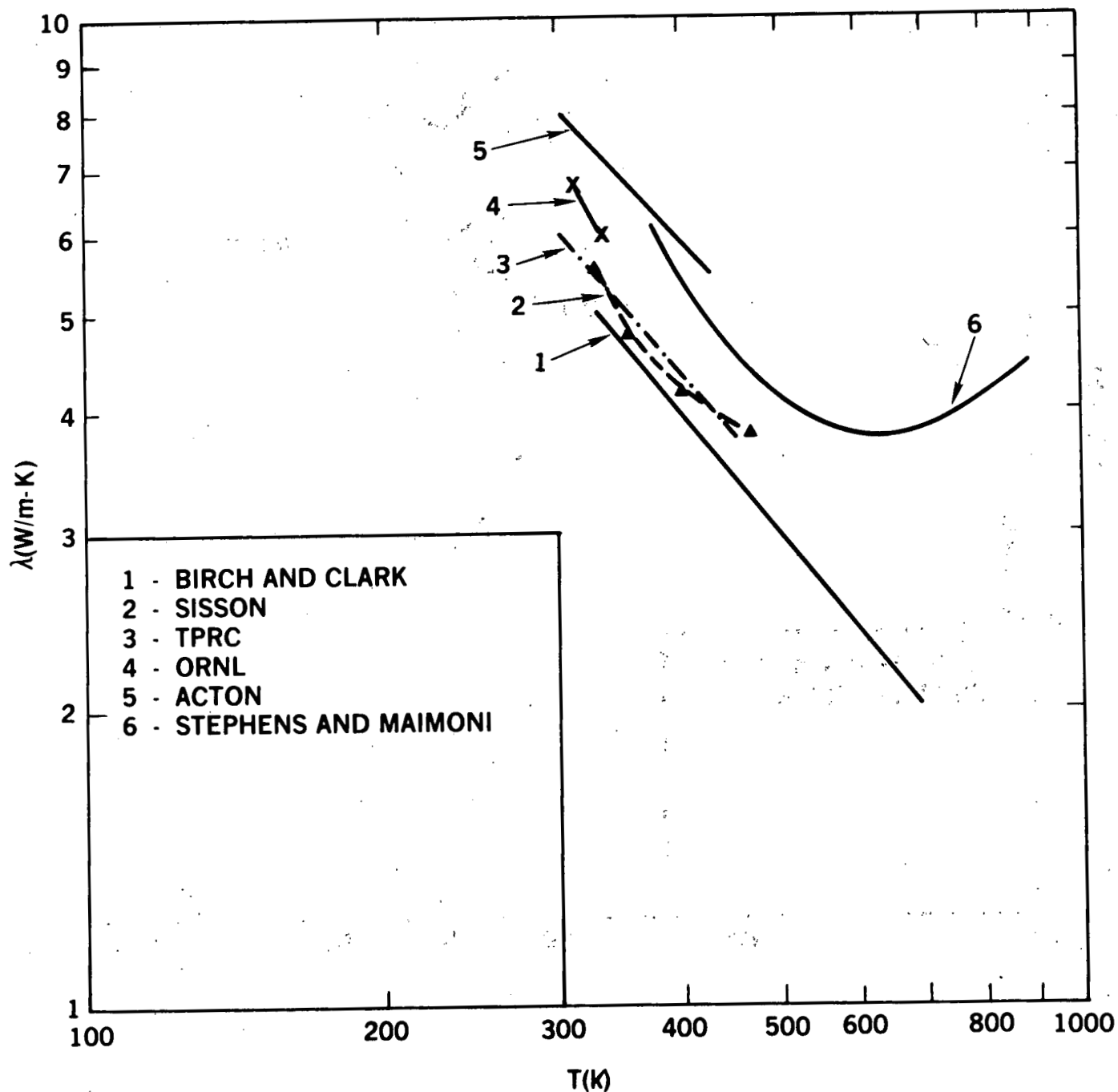


Fig. 9. Thermal Conductivity vs. temperature from various references: 1 - Birch and Clark (Ref. 9), 2 - Sisson (Ref. 29), 3 - TPRC (Ref. 20), 4 - ORNL (Ref. ), 5 - Acton (Ref. 5), 6 - Stephens and Maimoni (Ref. 23).

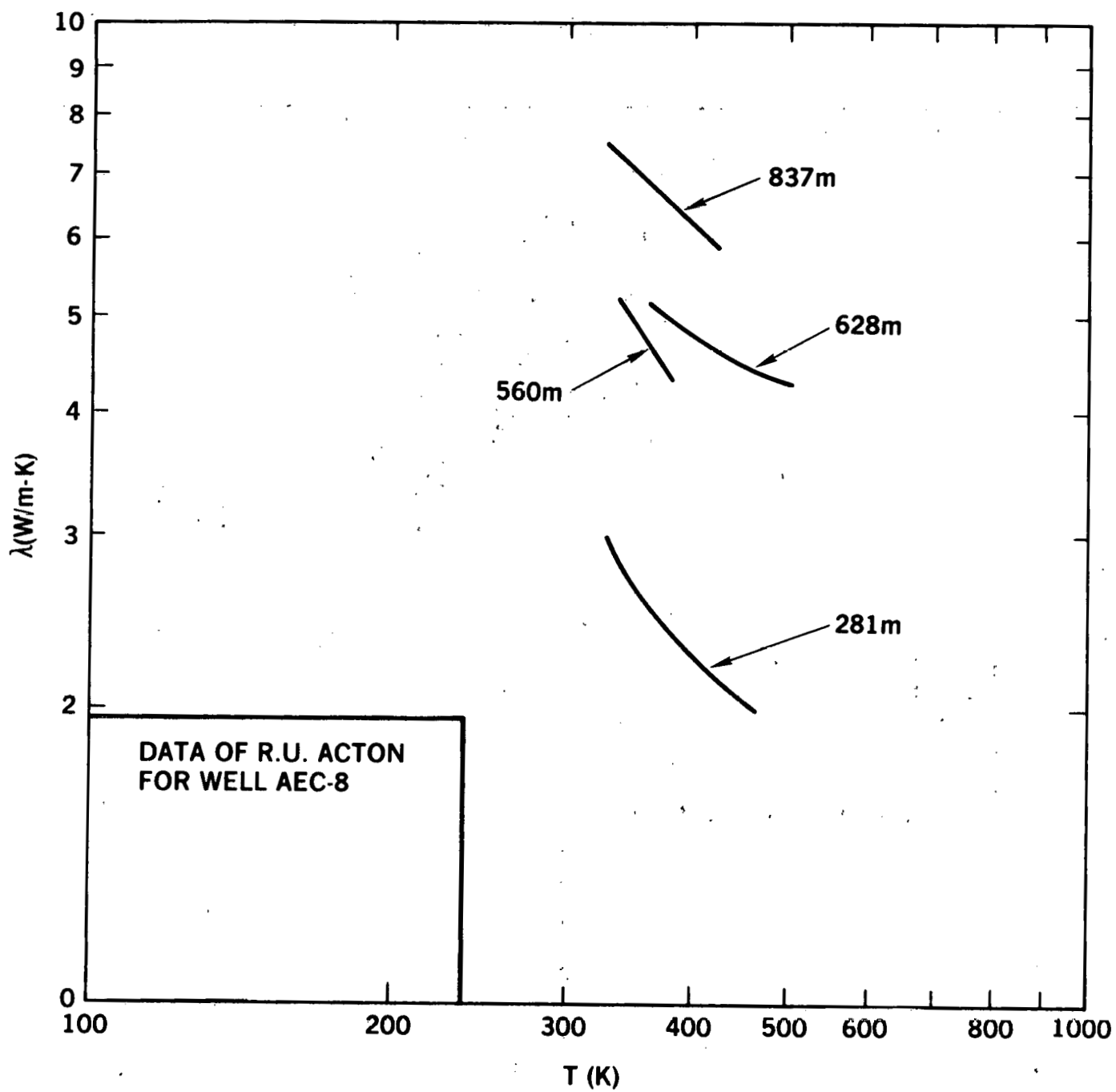


Fig. 10. Thermal conductivity vs temperature for samples from well AEC#8. Data of Acton (Ref. 5).

Some measurements on rocksalt conductivity which include radiative effects were reported by Stephens and Maimoni.<sup>23</sup> They used a radial heat flow technique on rocksalt samples from the Carey Mine, Winfield, LA. The samples were reported to be 99+% NaCl with small amounts of anhydrite ( $\text{CaSO}_4$ ) and were said to be translucent with many large crystals and aggregates of small crystals, some  $> 4$  in. in size. The smooth curve used by Stephens and Maimoni to represent their data is shown in Fig. 9. It is evident that the Stephens and Maimoni conductivity is higher than most of the data previously reported for rocksalt although it is less than that reported by Acton for the NM potash mine sample in the temperature region where both measurements overlap.

In summary of this review of past rocksalt thermal conductivity measurements, it may be noted that most of the reported data in the temperature range  $\sim 300$ - $600$  K is consistent with the form given by Eq. (5) and parameters  $\lambda_0 = 5$ - $6$  W/m-K and  $\gamma \approx 1.0$ - $1.2$ . The exceptions are one set of Acton data which has the Eq. (5) form but  $\lambda_0 = 8$  W/m-K and the Stephens and Maimoni data which exhibits radiative transport effects at temperatures above  $600$  K.

The major constituent present in most of the samples listed in Table I is halite and the second most prevalent mineral is anhydrite. Measurements of anhydrite conductivity as a function of temperature have not been previously reported. A number of  $293$  K conductivity measurements on anhydrite samples obtained from four different locations show conductivity values in the range  $4.9$ - $5.6$  W/m-K.<sup>31</sup> Since the temperature dependence of the conductivity is similar for most minerals which are electrical insulators, it is reasonable to assume that  $\lambda(T)$  for anhydrite is very similar to that of halite. In any future experimental thermal conductivity analysis of WIPP materials, it would be useful to determine the conductivity of anhydrite more precisely than was done in the experiments reported here, since anhydrite appears to be the predominate nonhalite mineral

present at typical WIPP site burial depths. It would also be useful to reexamine some polyhalite samples and to study the effect of water driveoff in more detail.

#### D. Conclusions on Thermal Conductivity Measurements

The major experimental result of this study is shown in the  $\lambda$  vs  $T$  graph of the Dynatech data, Fig. 5. For samples composed predominately of halite and/or anhydrite, the conductivity is described by Eq. (5) with  $\lambda_0$  in the range 4.5-5.5 W/m-K and  $\gamma = 1.14$ . The presence of other minerals or materials such as polyhalite or clay will result in a decrease in  $\lambda_0$  and a change in the temperature dependence of  $\lambda$ . The data is not extensive enough to allow any more detailed conclusions to be drawn.

The Sandia and Los Alamos conductivity measurements generally support the Dynatech results, although the Los Alamos measurements were made only over a limited temperature range and the Sandia measurements were subject to rather large sources of error. However, in no measurements in the present series were values of  $\lambda_0 > 6$  W/m-K observed. This is in contrast to the previous results of Acton<sup>5</sup> in which  $\lambda_0$  values as high as 8 W/m-K were reported.

The theory of insulator thermal conductivity generally supports the use of an expression of the form of Eq. (5) for describing the conductivity temperature dependence. The theoretical expressions given in Eq. (8) and Eq. (9) can predict the 300 K halite conductivity to within  $\sim 50\%$ . The small deviation of  $\gamma$  from unity in Eq. (5) is consistent with the presence of thermal expansion and optical phonon effects which are not included in the basic theory. Although deviations from the behavior predicted by Eq. (5) frequently were observed at temperatures  $T \gtrsim 500$  K, they were both positive and negative with respect to Eq. (5). Thus the measurements in this series do not positively confirm the predicted onset of radiative conductivity. This result is consistent with the infrared transmission measurements made by Bulmer on similar samples.

## V. Discussion of Thermal Conductivity Variation and its Effect on Repository Thermal Analysis

In a repository in which high level power producing waste is stored, the thermal conductivity of the material surrounding the waste will play a major role in determining the temperature in the vicinity of the waste containers. B. W. Bulmer has performed a sensitivity analysis using a one-dimensional transient numerical heat conduction analysis in order to determine the uncertainty in the maximum salt temperature as a function of the relative conductivity uncertainty.<sup>32,33</sup> This maximum temperature,  $T_{\max(s)}$ , occurs at the container-salt interface. Bulmer presents results showing  $\partial T_{\max(s)} / \partial \lambda_s$  vs  $\lambda_s$  and  $\Delta T_{\max(s)}$  vs.  $\Delta \lambda_s / \lambda_s$ , where  $\lambda_s$  = salt conductivity and  $\Delta T_{\max(s)}$  is the variation in  $T_{\max(s)}$  produced by an uncertainty  $\Delta \lambda_s$  in  $\lambda_s$ . In the transient case the temperature also depends on the thermal diffusivity,  $\alpha_s = \lambda_s / \rho C_p$ . Bulmer also gives results of calculating  $\Delta T_{\max(s)}$  vs.  $\Delta C_p / C_p$ .

It is possible to demonstrate analytically the dependence of  $\Delta T_{\max(s)}$  on  $\lambda_s$  using representative solutions of the heat conduction equation for simplified model problems. In the situation modeled by Bulmer, the waste is considered as a distributed medium in a slab geometry. For a very simplified analysis, we consider the steady state problem in which a waste slab of thickness  $L$  and conductivity  $\lambda_w$  produces heat at a rate  $\dot{p}$  per unit volume, with the heat being conducted to sinks on either side at a temperature  $0^\circ\text{C}$  and located a distance  $\delta$  from the waste slab edge as shown in Fig. 11. The one dimensional steady state heat conduction equation, for temperature independent  $\lambda_s$  and  $\lambda_w$  is,

$$\frac{d^2 T(z)}{dz^2} + \dot{p}(z) / \lambda_{s,w} = 0 \quad (16)$$

The solution of Eq. (16) which satisfies the boundary conditions is,

$$T(z) = \begin{cases} (\dot{p}L(2\lambda_w) \left\{ [L/4 + (\lambda_w/\lambda_s)(\delta - L/2)] - z^2 \right\}) ; 0 < z \leq L/2 \\ (\dot{p}L/2\lambda_s)(\delta - z) ; L/2 < z \leq \delta \end{cases} \quad (17)$$

From the second of Eq. (17),  $T_{\max(s)} = T(L/2)$ , or,

$$\begin{aligned} T_{\max(s)} &= (\dot{p}L/2\lambda_s)(\delta - L/2) \\ &\approx \dot{p}L\delta/2\lambda_s \end{aligned} \quad (18)$$

for  $\delta \gg L/2$ . Although the expression for  $T_{\max(s)}$  in Eq. (18) contains the arbitrary length  $\delta$ , it does show that  $T_{\max(s)}$  is inversely proportional to  $\lambda_s$ , or

$$\partial T_{\max(s)} / \partial \lambda_s = -T_{\max(s)} / \lambda_s \quad (19)$$

Using the results of Sisson's analysis,<sup>29</sup>  $T_{\max(s)} \lesssim 100$  C and thus,

$$\Delta T_{\max(s)}(C) \lesssim 100 (\Delta \lambda_s / \lambda_s) \quad (20)$$

In the case of the medium being composed of rocksalt and/or anhydrite, we have seen from the data in Sec. IV-B that  $\Delta \lambda_s / \lambda_s \sim 0.2$ , and hence,  $\Delta T_{\max(s)} \lesssim 20$  C.

For a somewhat more realistic analysis, we consider a thin slab source dissipating power into an infinite medium as shown in Fig. 12. If the source of heat flux is turned on at time  $t = 0$  with a constant strength  $F_o$  ( $W/m^2$ ), then the temperature as a function of time and distance  $z$  from the source plane is given by,<sup>34</sup>

$$T(z, t) = \frac{2F_o}{\lambda_s} \left\{ \left( \frac{\alpha_s t}{\pi} \right)^{1/2} \exp[-z^2/4\alpha_s t] - (z/2) \operatorname{erfc}[z/2(\alpha_s t)^{1/2}] \right\} \quad (21)$$

where  $\operatorname{erfc}$  is the complementary error function. The maximum temperature in the medium surrounding the source occurs at  $z = 0$ , and from Eq. (21) is given by,



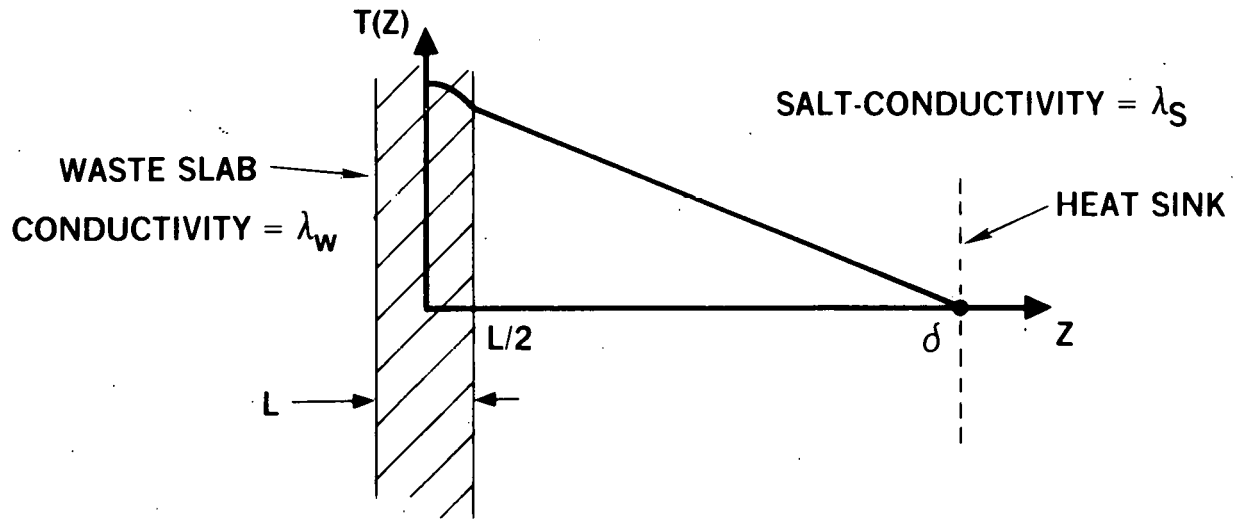


Fig. 11. Waste slab of thickness  $L$  producing heat at a rate  $p(\text{W/m}^3)$  which is conducted to two heat sinks each located a distance  $\delta$  from the slab edges and maintained at a temperature of  $0^\circ\text{C}$ . The problem is symmetrical with respect to the centerline,  $z = 0$ .

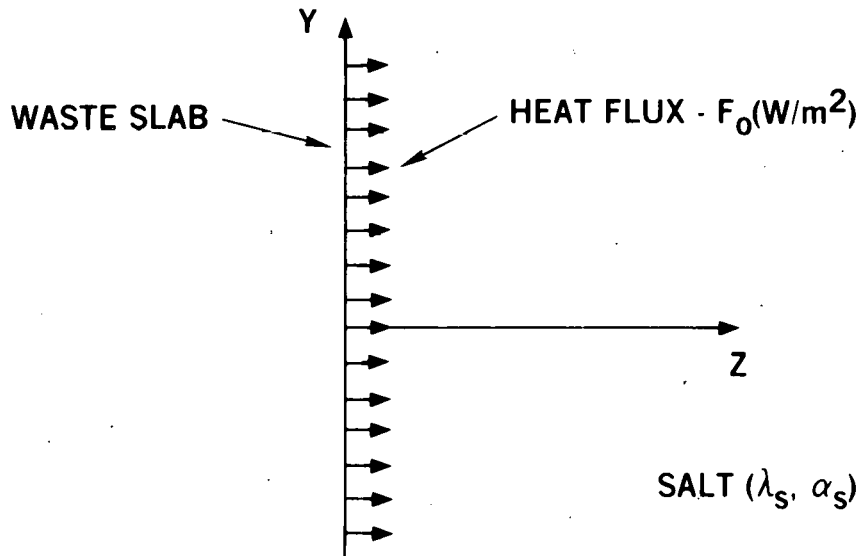


Fig. 12. Uniform planar flux source located at  $z = 0$  dissipating power  $2F_0$  ( $\text{W/m}^2$ ) into two uniform infinite half spaces.

$$T(0,t) = \frac{2F_o}{\lambda_s} \left( \frac{\alpha_s t}{\pi} \right)^{1/2} \quad (22)$$

In this case, with  $F_o$  independent of time,  $T_{\max}(s) = T(0,t)$  depends on  $\lambda_s$  as  $\lambda_s^{-1/2}$ , since  $\alpha_s = \lambda_s / \rho C_p$ .

In the case of a time dependent source of flux  $F(t)$  which is turned on at  $t = 0$ , the time dependent temperature is given by the convolution integral,<sup>34</sup>

$$T(z,t) = \frac{\alpha_s^{1/2}}{\lambda_s \pi^{1/2}} \int_0^t \frac{F(t - t_o)}{t_o^{1/2}} \exp(-z^2 / 4\alpha_s t_o) dt_o \quad (23)$$

Eq. (23) exhibits the same dependence on  $\alpha_s$  and  $\lambda_s$  that the solution for constant heat flux, Eq. (21) shows. It is interesting to note that the analytical solution in Eq. (23) can be easily used to derive information about the time dependent variation of  $T_{\max}(s)$  for an exponentially decaying heat flux source of the type used by Bulmer<sup>32</sup> and Sisson<sup>29</sup> in numerical thermal response calculations. Bulmer analyzed the one dimensional conduction problem using a source of the type,

$$F(t) = F_o \exp(-t/\tau) \quad , \quad (24)$$

where  $\tau = 38.95$  y corresponding to a 27y half life ( $t_{1/2} = 0.693\tau$ ). Sisson analyzed two and three dimensional problems with the aid of the CINDA heat transfer code, using a source given approximately by Eq. (24). The biggest variation between Sisson's source and Eq. (24) occurs for  $t \approx 8y$  where Sisson's source is about 5% higher than that calculated from Eq. (24). For  $t \gtrsim 28y$  both sources are essentially identical.

Eq. (23) for  $T(z,t)$  with  $F(t)$  given by Eq. (24) is,

$$T(z,t) = \frac{\alpha_s^{1/2} F_o e^{-t/\tau}}{\lambda_s \pi^{1/2}} \int_0^t \exp[t_o/\tau - z^2/4\alpha t_o] \frac{dt_o}{t_o^{1/2}} \quad (25)$$

At  $z = 0$ ,  $T_{\max}(s) = T(0,t)$  is

$$T(0,t) = \frac{\alpha_s^{1/2} F_o e^{-t/\tau}}{\lambda_s \pi^{1/2}} \int_0^t \exp(t_o/\tau) \frac{dt_o}{t_o^{1/2}} \quad (26)$$

By making a series expansion of the exponential, the integral in Eq. (26) may be evaluated to yield,

$$T(0,t) = \frac{2F_o (\alpha_s t)^{1/2} e^{-t/\tau}}{\lambda_s \pi^{1/2}} M(1/2, 3/2, t/\tau) \quad , \quad (27)$$

where  $M$  is Kummer's function of its arguments,<sup>35</sup> defined in our specific case as,

$$M(1/2, 3/2, t/\tau) = \sum_{n=0}^{\infty} \frac{1}{n!} \frac{1}{(2n+1)} \left(\frac{t}{\tau}\right)^n \quad (28)$$

In the limiting case  $t \ll \tau$ ,  $M \approx 1$  and  $T(0,t) \propto t^{1/2} \exp(-t/\tau)$  while for  $t \gg \tau$ ,  $M = (1/2)(\tau/t)\{1 + 1/[2(\tau/t)] + 1/[4(\tau/t)^2] + \dots\} \exp(t/\tau)$ , and thus  $T(0,t) \propto t^{-1/2}$  at long times. The function  $t^{1/2} \exp(-t/\tau)$  has a maximum at  $t = \tau/2$ . The presence of the  $M$  function factor in Eq. (27) tends to shift the maximum to somewhat longer times.  $T(0,t)$  from Eq. (27) is shown graphically in Fig. 13, plotted as  $T(0,t)/[2F_o(\alpha_s \tau)^{1/2}/\lambda_s \pi^{1/2}]$  vs.  $t/\tau$ . The maximum occurs at  $t \approx 0.85 \tau$  where  $T_{\max}(s)$  satisfies the relation.

$$T_{\max}(s) = 0.54 \left[ \frac{2F_o}{\lambda_s \pi^{1/2}} (\alpha_s \tau)^{1/2} \right] \quad (29)$$

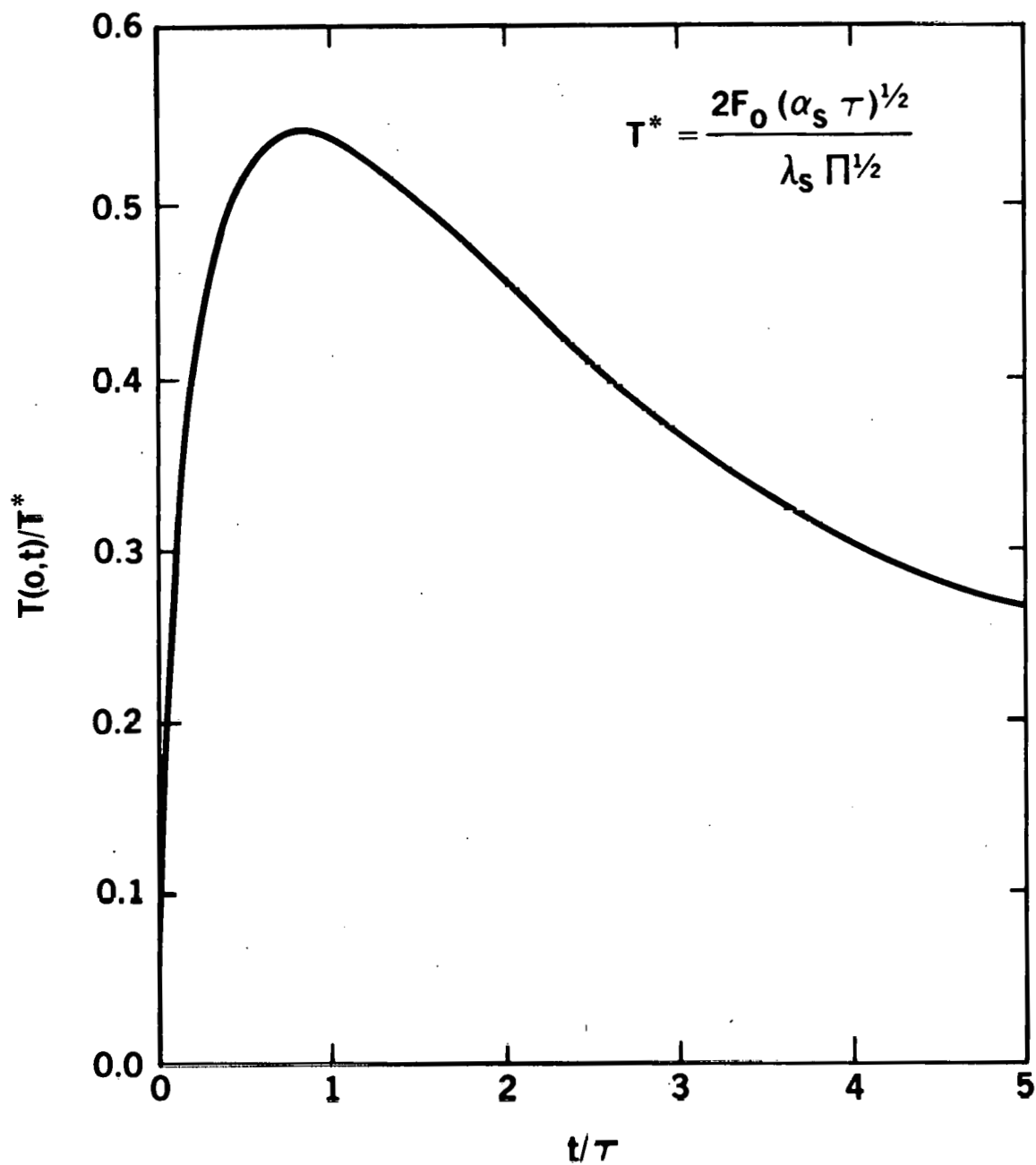


Fig. 13. Temperature vs time at the plane  $z = 0$  produced by a heat source decaying exponentially with a half-life  $t_{1/2} = 0.693\tau$ . Time is measured in units of  $\tau$  and temperature in units of  $2F_0(\alpha_s \tau)^{1/2}/\lambda_s \pi^{1/2}$ .

To compare the estimated maximum salt temperature found from Eq. (29) with Sisson's numerical calculations, a realistic value of  $F_0$  needs to be determined. The geometry considered by Sisson is shown in Fig. 14. Three rows of 300 W canisters, each 10 ft long and 2 ft in diameter are located in a drift region, with a 100 ft spacing between drift region centerlines. The canisters are located on a square lattice in a horizontal plane with a lattice spacing of 5 ft. The thermal properties assumed for this calculation are shown in Table VIII.

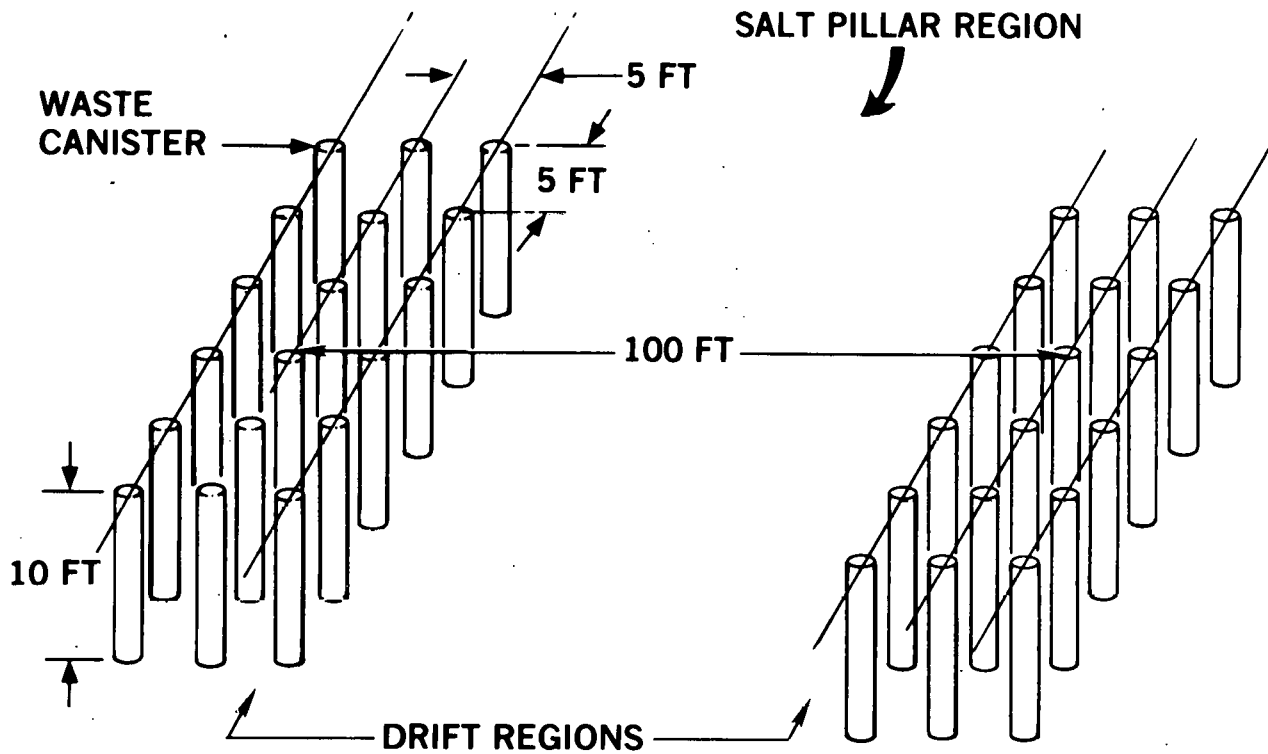
---

Table VIII  
Salt Thermal Properties Used for Model Calculations

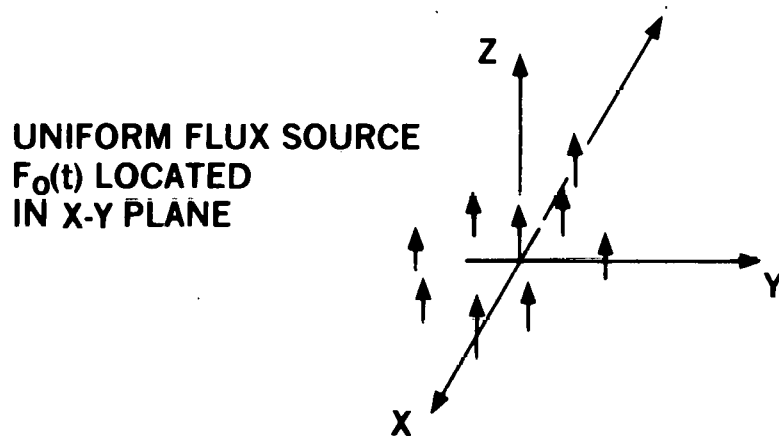
<u>Property</u>	<u>Value</u>
Density - $\rho$	2160 kg/m <sup>3</sup>
Specific Heat - $C_p$	887.6 J/kg-°K
Thermal Conductivity - $\lambda_s$	4.5 W/m-K
Thermal Diffusivity - $\alpha_s$	$2.35 \times 10^{-6}$ m <sup>2</sup> /s

---

The density and specific heat are those used by Sisson, while the conductivity is an estimated average value, corresponding to that calculated from Eq. (5), for  $\lambda_s = 5.5$  W/m-K, and  $T = 350$  K. The thermal wave originating from the waste canisters will reach a point  $y$  half way between drift spaces in a time  $t \sim z^2/4\alpha_s$ . For  $z = 50$  ft, that time is  $t \sim 0.8y$ . Thus, at a time  $t \sim .85\tau \approx 33y$  it is reasonable to assume that the region near  $z = 0$  between drift spaces is essentially at thermal equilibrium and in an isothermal state. the sources can then be smeared out as shown in Fig. 13(b) to form a plane source in the  $x$ - $y$  or horizontal plane. The source density  $2F_0$  is then  $(300 \text{ W/canister})(3 \text{ canisters})/(500 \text{ ft}^2) = 1.8 \text{ W/ft}^2$  (78.4 kW/acre) or  $19.38 \text{ W/m}^2$ , as given by Sisson (Fig. 2 of Ref. 29). The value of  $T_{\max(s)}$  found from Eq. (29) with this source is,  $T_{\max(s)} = 70.4$  C. Sisson's calculation predicts  $T_{\max(s)} = 85$  C at a time  $\approx 23y$  (Fig. 9 of Ref. 29), with



(a)



(b)

Fig. 14. (a) Burial scheme for waste in a high-level waste repository. Rows of canisters are buried in drift regions separated by salt pillars. The pillar spacing is determined by the maximum areal power density permitted. (b) Smeared out heat source in the x-y plane at  $z = 0$  producing a uniform heat flux  $F_0(t)$  into each half space.

the temperature half way between the drift spaces being  $\approx 55$  C at this time. Thus, our assumption of an isothermal source in the x-y plane is only approximately true. Nevertheless, Eq. (29) does yield a result on the same order as the numerical result and also demonstrates explicitly the dependence on  $T_{\max(s)}$  on  $\alpha_s$  and  $\lambda_s$ . Sisson's numerical temperature vs. time results (Fig. 9 of Ref. 24) have a shape which is qualitatively similar to that shown in Fig. 13. The temperature at nodes close to a fuel element tends to rise somewhat faster at short times and the maximum temperature occurs at  $\sim 0.6 t_0$  in the numerical calculation. However, the maximum is very broad in the numerical result as it is in Fig. 10.

The major result of this analysis is that dependence of maximum temperature on thermal conductivity goes as,

$$T_{\max(s)} = k\lambda_s^{-x} \quad , \quad (30)$$

where  $0.5 \leq x \leq 1$ , depending on the exact boundary conditions and the variations in  $\rho$  and  $C_p$  which accompany variations in  $\lambda_s$ . The variation in maximum temperature  $\Delta T_{\max(s)}$  produced by a variation  $\Delta \lambda_s$  in thermal conductivity is then estimated by,

$$\Delta T_{\max(s)} = -x T_{\max(s)} \left( \frac{\Delta \lambda_s}{\lambda_s} \right) \quad . \quad (31)$$

Considering a 50% variation in  $\lambda_s$ , with  $T_{\max(s)} = 100$  C and  $x = 0.75$ , Eq. (31) yields  $\Delta T_{\max(s)} = 38$  C, in good agreement with the results of Bulmer's numerical analysis. The data on salt thermal conductivity shown in Fig. 5 indicate that all specimens which were composed principally of rocksalt and/or anhydrite or polyhalite had conductivities in the range 3-6 W/m-K, and thus, for the assumed waste power density (78 kW/acre), the uncertainty in maximum salt temperature should be  $< 40$  C.

## VI. Discussion and Conclusions

Discussions of the major conclusions of this study are contained in the final parts of Secs. II, III and IV for specific heat, thermal expansion, and thermal conductivity, respectively. Thus, this section will be devoted to more general observations and suggestions for future work. Due to the very heterogeneous nature of the rocksalt at or near the WIPP site, it is impossible in any finite experimental program to completely characterize this material. Nevertheless, measurements of the sort reported in this study do indicate trends which can be used as an aid in choosing parameters for thermal or thermal-mechanical modeling of a repository.

In the case of specific heat, we feel that this parameter can be calculated to sufficient accuracy if the identity and volume fractions constituents in the region under consideration are known. For regions in which the material is  $\geq 90\%$  halite, the pure NaCl specific heat (Table II) is very close to that of the actual material. In any future experimental program, it is recommended that the specific heats of polyhalite and anhydrite be measured, since these are the principal non-halite minerals present in the rocksalt.

In the case of thermal expansion, the results shown in Fig. 1 indicate that, for small samples, the measured linear expansion is characteristic of that of the major constituent of the sample. In these experiments, samples composed predominantly of halite, polyhalite, anhydrite, and gypsum were measured. The expansion coefficients of the samples with halite as the major constituent were close to that reported for pure NaCl, while the expansion coefficients for anhydrite or polyhalite samples were about half that of NaCl. On the basis of this limited set of measurements, we recommend using  $\bar{\alpha}$  values (in units of  $10^{-6} \text{ K}^{-1}$ ) of 45, 27 and 20 for halite, polyhalite and anhydrite, respectively. If any future thermal expansion measurements are performed, it is recommended that more halite



and polyhalite samples be measured, and possibly that techniques be devised for measuring the expansion of larger and more heterogeneous samples.

The major result of the thermal conductivity studies is that the conductivity of samples composed largely of halite and/or anhydrite is governed by Eq. (5) with  $\lambda_0$  in the range 4.5-5.5 W/m-K and  $\gamma = 1.14$ . Significant concentrations of polyhalite will result in a lowering of  $\lambda_0$  and possibly a shift in  $\gamma$ . The sensitivity of maximum salt temperature to variations in  $\lambda$  is estimated to be such that a 50%  $\lambda$  variation will produce a resultant temperature variation  $< 40$  C for nominal waste burial densities. On the basis of our experiments, we conclude that  $\lambda$  is known to within about 50% for regions composed predominately of halite, polyhalite and anhydrite. The data in Fig. 5 support the conclusion that  $\lambda_0$  falls in the range 1.5-6 W/m-K for all samples measured which were composed largely of these three minerals. As in the specific heat and expansion measurements, it would be desirable to do more measurements of polyhalite and anhydrite samples if any future experimental program is undertaken.

#### Acknowledgements

We would like to thank H. P. Stephens and T. V. Torney for performing the specific heat measurements.

#### References

1. J. N. Sweet, J. E. McCreight, "Thermal Conductivity of Rocksalt and Other Geologic Materials from the Site of the Proposed Waste Isolation Pilot Plant," 16th International Thermal Conductivity Conference, IITRI, Chicago, IL, Nov. 7-9, 1979, to be published in conference proceedings and Sandia Internal Report, SAND 79-1665, Dec. 1979.\*
2. D. W. Powers, et al. (editors), "Geological Characterization Report, Waste Isolation Pilot Plant (WIPP) Site Southeastern New Mexico," Sandia Report, SAND 78-1596, 1978, Vols. I-II.\*

3. D. R. Stull, H. Prophet, JANAF Thermochemical Tables, 2nd Ed., Office of Standard Reference Data, NBS, Wash., DCC, 20234, 1971.
4. Y. S. Touloukian, et al., Thermal Expansion - Nonmetallic Solids, Thermophysical Properties of Matter, Vol. 13, IFI Plenum, NY, 1977, p. 1000.
5. R. U. Acton, "Thermal Conductivity of S. E. New Mexico Rocksalt and Anhydrite," in Thermal Conductivity 15, Ed. by V. V. Mirkovich (Proceedings of the 15th International Conference on Thermal Conductivity) Plenum Press, NY, 1978, pp. 263-276.
6. J. G. Dodson, LASL, personal communication.
7. S. Spinney, "The Thermal Conductivity of Fifteen Salt Core Specimens," Dynatech R/D Co. Report No. SAD-15, contract 13-0164, 1979 (see Appendix B).
8. M. J. Laubitz, "Measurement of the Thermal Conductivity of Solids at High Temperatures by Using Steady-State Linear and Quasi-Linear Heat Flow," in R. P. Tye (Ed), Thermal Conductivity, Vol. I, Academic Press, NY, 1969, pp. 111-183.
9. F. Birch, H. Clark, "The Thermal Conductivity of Rocks and Its Dependence Upon Temperature and Composition, Part II," Am. J. Sci. 238, 613 (1940).
10. P. G. Klemens, "Thermal Conductivity and Lattice Vibrational Modes," in Solid State Physics Vol VII, Ed. by F. Seitz, D. Turnbull, Academic Press Inc., NY, 1958, pp. 1-97.
11. P. G. Klemens, "Theory of the Thermal Conductivity of Solids," in Thermal Conductivity Vol I, Ed. by R. P. Tye, Academic Press, NY, 1969, pp. 1-68.
12. J. M. Ziman, Electrons and Phonons, Oxford, London, 1960, pp. 128-156, 288-326.
13. G. A. Slack, "The Thermal Conductivity of Nonmetallic Crystals," in Solid State Physics Vol 34, Ed. by F. Seitz and D. Turnbull, Academic Press, NY, 1979, pp. 1-71.

14. G. Leibfried, E. Schlomann, Nachr, Akad. Wiss Gottingen; Math Phys Kl, 4, 71 (1954).
15. J. E. Parrott, A. D. Stuckes, Thermal Conductivity of Solids, Pion Ltd., London, 1975, pp. 114-116.
16. Ref. 13, p. 12, Eq. (3.3) and p. 43, Eq. (12.5).
17. Ref. 13, pp. 37-44.
18. C. Kittel, Introduction to Solid State Physics, 4th Ed. John Wiley, NY, 1971, p. 27.
19. N. W. Ashcroft, N. D. Mermin, Solid State Physics; Holt, Rinehart and Winston, NY, 1976, p. 494.
20. TPRC Data Series - Vol II, Thermal Conductivity of Nonmetallic Solids, Y. S. Touloukian Ed., IFI/Plenum, NY, 1970, p. 621.
21. Ref. 18, pp. 224-225.
22. Ref. 11, p. 50.
23. D. R. Stephens, A. Maimoni, "Thermal Conductivity of Rocksalt," UCRL-6894, Rev. II, Univ. of Calif. Lawrence Radiation Laboratory, Livermore, CA, 1964.
24. R. Viskanta, E. E. Anderson, "Heat Transfer in Semitransparent Solids," in Advances in Heat Transfer Vol. 11, Ed. by T. F. Irvine, Jr. and J. P. Hartnett, Academic Press, NY, 1975, pp. 317-441.
25. Ref. 16, p. 333.
26. Electro-Optics Handbook, RCA, Harrison, NJ, 1968, p. 4-4.
27. B. W. Bulmer, Sandia Laboratories, to be published.
28. R. D. Cheverton, W. D. Turner, "Thermal Analysis of the National Radioactive Waste Repository: Progress Through June 1971," Oak Ridge National Laboratory Report ORNL-4726, Contract No. W-7405-eng-26, Dec. 1971.\*
29. C. E. Sisson, "Predicted Temperatures in a Bedded-Salt Repository Resulting from Burial of DOE High-Level Nuclear Waste Containers," Sandia Report SAND-78-0924, 1978.\*

30. Dave McElroy, ORNL, private communication and ORNL Drawing - DWG 71-11031.
31. S. P. Clark, Jr. (Ed.), Handbook of Physical Constants, Geological Society of America Inc., Memoir 97, 1966, p. 463.
32. Sandia memo; B. M. Bulmer (1261) to J. R. Wayland (5311), "Thermal Properties Sensitivity in Geologic Media Surrounding Buried Heat Sources," Feb. 28, 1978.
33. Sandia memo; B. M. Bulmer (1261) to J. R. Wayland (5311), "Thermal Properties Sensitivity Studies," April 3, 1978.
34. H. C. Carslaw and J. C. Jaeger, Conduction of Heat in Solids, 2nd Ed., Oxford Univ. Press, London, 1959, pp. 75-76.
35. M. Abramowitz, I. A. Stegun, Handbook of Mathematical Functions, Dover Publications, NY, 1965, p. 504.

Appendix A



Report On  
THE LINEAR THERMAL EXPANSION  
OF SALT AND ROCK CORE  
SPECIMENS

Prepared For:

Sandia Laboratories  
Albuquerque, New Mexico 87115

Dynatech Report No. SAD-15  
Work Carried Out Under Contract No. 13-0164

Submitted by:



Stewart C. Spinney  
Manager  
Thermophysical Properties Testing



# DYNATECH

Report On  
THE LINEAR THERMAL EXPANSION  
OF SALT AND ROCK CORE  
SPECIMENS

Fifteen salt core specimens were submitted for analysis of the linear thermal expansion. The core specimens were cored from salt caverns in New Mexico in order to study the thermal properties necessary to model the caverns for storage of nuclear waste materials.

The fifteen core samples were submitted as cylinders, thirteen of the cylinders were 108 mm diameter and two were 64 mm diameter. The specimens AEC and ERDA were 108 mm diameter and the specimens designated WIPP were 64 mm diameter. All specimens were approximately 250 mm long.

From the submitted materials, specimens approximately 50 mm x 12 mm x 12 mm were saw cut for use as test samples. The samples were sealed in a desiccator with activated desiccant prior to test.

## Experimental Procedure

The initial length of the sample was accurately measured with a micrometer. The specimen was then instrumented in the quartz measuring head of a Netzsch Electronic Automatic Recording Dilatometer. The system was placed at the center zone of an environmental chamber and programmed for temperature rise and equilibration points. During the entire experiment, the length and temperature of the specimens were recorded continuously, autographically.



**DYNATECH**

The data was evaluated as follows:

$$T_e = \frac{\Delta L}{L_o}$$

Where  $T_e$  = thermal expansion

$\Delta L$  = the total change in length from 293k to each temperature point, T

$L_o$  = initial length at 293k

The results for the samples tested are given in the following table.

TABLE

THE LINEAR THERMAL EXPANSION OF  
SALT AND ROCK CORE SPECIMENS

Sample Reference	Linear Thermal Expansion $10^4 \Delta L/L_0$						Overall Coefficient Of Linear Thermal Expansion $10^{-6} \text{degK}^{-1}$
	293K	300K	400K	500K	600K	700K	
1 2703.5-8 to 2704.7-8	0	2.6	44.3	85.9	127.6	(2)	41.6
2 2055.3-8 to 2056-8	(1)						
3 ERDA 9/2840.7 to 2841.45	(1)						
4 ERDA 9/1908 to 1908.75	0	2.5	46.3	90.2	134.1	(2)	43.7
5 ERDA 9/1910.3 to 1910.9	0	1.3	29.7	58.2	86.6	115.1	28.3
6 ERDA 9/1631.4 to 1632	0	0.4	20.9	41.5	62.0	82.6	20.3
7 ERDA 9/1086.8 to 1087.55	0	1.3	44.0	86.8	129.5	(2)	42.2
8 ERDA 9/1969.4 to 1970.1	0	2.3	49.6	96.8	144.1	(2)	46.9
9 AEC #8MB133/2001.9 to 2002.7	0	1.5	27.2	52.8	78.5	104.2	25.6
10 AEC #8/1995.6 to 1996.1	0	1.8	27.8	(2)	(2)	(2)	26.0
11 AEC #8/698 to 698.5	0	2.0	30.8	(2)	(2)	(2)	28.8
12 AEC #8/1212.25 to 1213.1	0	1.3	44.4	87.6	130.1	(2)	42.4
13 AEC #8/2062.6 to 2063.2	0	2.1	47.2	92.2	137.3	(2)	44.7
14 WIPP19/616 to 617	0	1.9	27.6	(2)	(2)	(2)	25.8
15 WIPP19/267.35 to 268.35	0	0.1	12.7	25.6	38.4	51.2	12.6

(1) Samples suitable for measurement could not be obtained from the core material.

(2) Sample decomposed.




Appendix B

THE THERMAL CONDUCTIVITY  
OF FIFTEEN SALT CORE SPECIMENS

Prepared for:  
Sandia Laboratories  
Albuquerque  
New Mexico 87115

Dynatech Report No. SAD-15  
Work Carried Out Under Contract Number 13-0164

Submitted by: 

Stewart C. Spinney, Manager  
Thermophysical Properties Testing

Report on

THE THERMAL CONDUCTIVITY  
OF FIFTEEN SALT CORE SPECIMENS

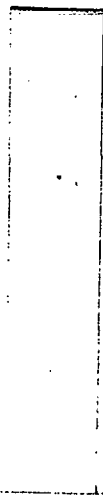
1. Introduction

Fifteen salt core specimens were submitted for analysis of the thermal conductivity. The core specimens were cored from salt caverns in New Mexico in order to study the thermal properties necessary to model the caverns subsequent to storage of nuclear waste materials.

2. Sample Description and Preparation

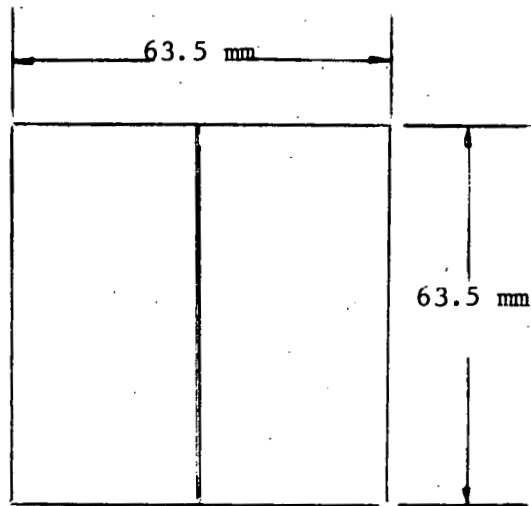
The fifteen core samples were submitted as cylinders, thirteen of the cylinders were 108 mm diameter and two were 64 mm diameter. The specimens AEC and ERDA were 108 diameter and the specimens designated WIPP were 64 mm diameter. All specimens were approximately 250 mm long.

From the 108 mm diameter material, specimens 64 x 64 x 12 mm were prepared, and from the 64 mm diameter material, specimens 51 mm diameter were prepared. Figures 1 and 2 show the specimen configurations.



Reference: SAD-15

January, 1979



NOTES:

- 1) Grooves across both faces  
0.51 x 0.51 mm

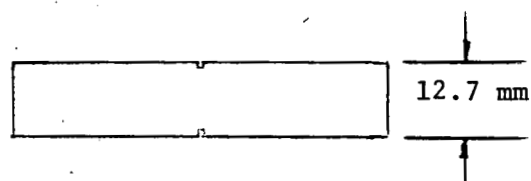


Fig. 1 Specimen Configuration Cut From 108 mm Diameter Cores

- 2) Specimens Flat and Parallel  
to 0.025 mm

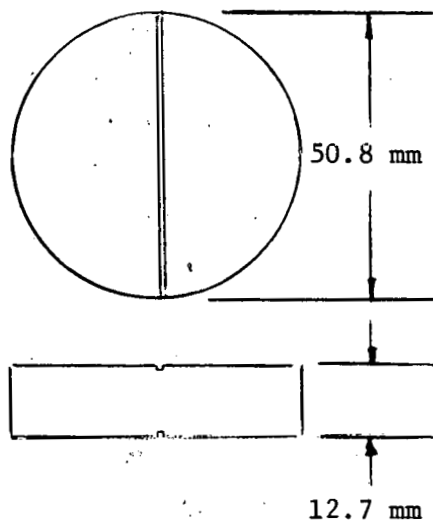


Fig. 2 Specimen Configuration Cut From 64 mm Diameter Core.

Reference: SAD-15

January, 1979

The specimens were prepared by first cutting slices of the core about 19 mm thick using a metal bonded segmented diamond wheel. Then one surface was made flat with a free abrasive lap, dry. Both surfaces were made flat and parallel to tolerance using a small vitrified stone wheel surface grinder. The edges of the specimen were then prepared by slicing using a resin bonded carbide wheel and then a stone wheel. The preparation efficiency was approximately 80% which was considered excellent considering the nature of the samples.

The prepared samples were stored until test in a desiccator containing activated  $\text{CaCl}_2$  as a desiccant.

### 3. Measurement Theory

The method of measurement chosen was the flat slab comparative technique. From Fourier's heat conduction equation the following equation is obtained.

$$\lambda = \left( \frac{q}{A} \right) \left( \frac{x}{\Delta T} \right)$$

where  $\lambda$  = thermal conductivity

$q$  = heat flow or energy transfer per time

$A$  = cross sectional area through which the energy flows

$x$  = thickness across which energy flows

$\Delta T$  = temperature difference created by energy flow across distance  $x$

If two materials having the same cross sectional area are stacked together have a temperature gradient established through them at equilibrium and have radial heat loss prevented by a system of guarding, then the heat flux, the  $q/A$ , through each of them must be the same. This arrangement is shown in the stack diagram of Figure 3.

Reference: SAD-15

January, 1979

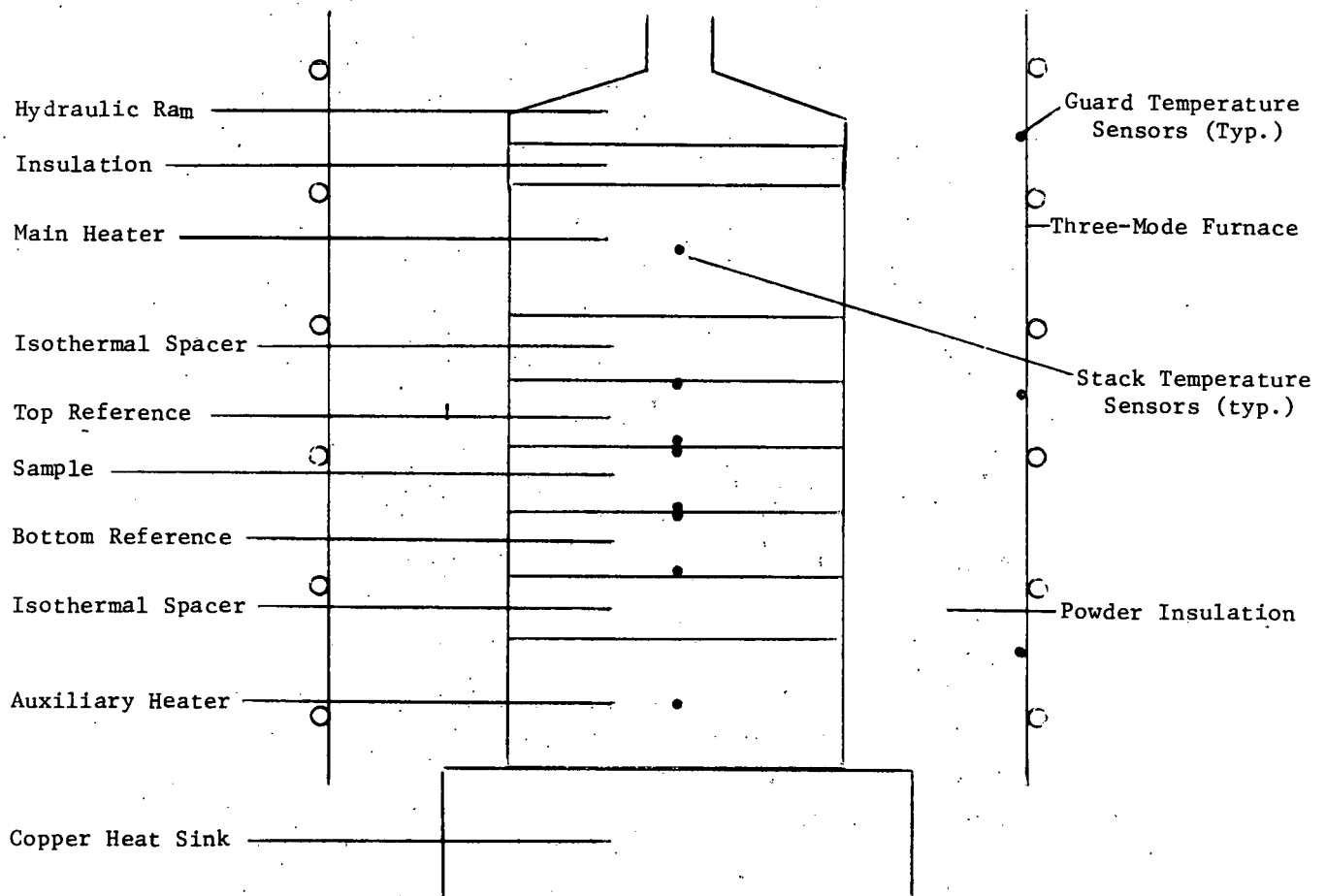


Fig. 3 Stack Diagram

Equation (1) can be rearranged to

$$\frac{q}{A} = \frac{\lambda \Delta T}{x} \quad (2)$$

$$\left( \frac{\lambda \Delta T}{x} \right)_1 = \left( \frac{\lambda \Delta T}{x} \right)_2 \quad (3)$$

Reference: SAD-15

January, 1979

and

$$\lambda_1 = \left( \frac{x}{\Delta T} \right)_1 \left( \frac{\lambda \Delta T}{x} \right)_2 \quad (4)$$

In practice the comparative technique sandwiches the unknown specimen between two reference materials of known thermal conductivity then one reference measures the heat flux into the specimen and the other measures the heat flux out of the specimen - the heat flux from the two references are averaged to obtain the average heat flux through the specimen.

The equation used to calculate the thermal conductivities is

$$\lambda_s = \left( \frac{1}{2} \right) \left( \frac{x}{\Delta T} \right)_s \left( \left( \frac{\lambda \Delta T}{x} \right)_R + \left( \frac{\lambda \Delta T}{x} \right)_r \right) \quad (5)$$

where  $\lambda$  = thermal conductivity  
 $x$  = distance or thickness across which temperature is measured  
 $\Delta T$  = temperature difference across distance  $x$   
 $s$  = sample parameters  
 $R$  = reference parameters  
 $r$  = reference parameters

The three factors which control the accuracy of the comparative method to the greatest degree are the temperature guarding, the contact resistance between the sample and references and the match of the thermal conductivity of the references and sample.

The temperature guarding is created by a three-mode furnace which uses three separate heater windings and three separate sensors which control the operation of electronic temperature controls. Using this guarding technique, a close match is possible between the stack temperature gradient and the guard temperature gradient. In addition, the interspace between the stack and guard is filled with a low thermal conductivity insulating powder.

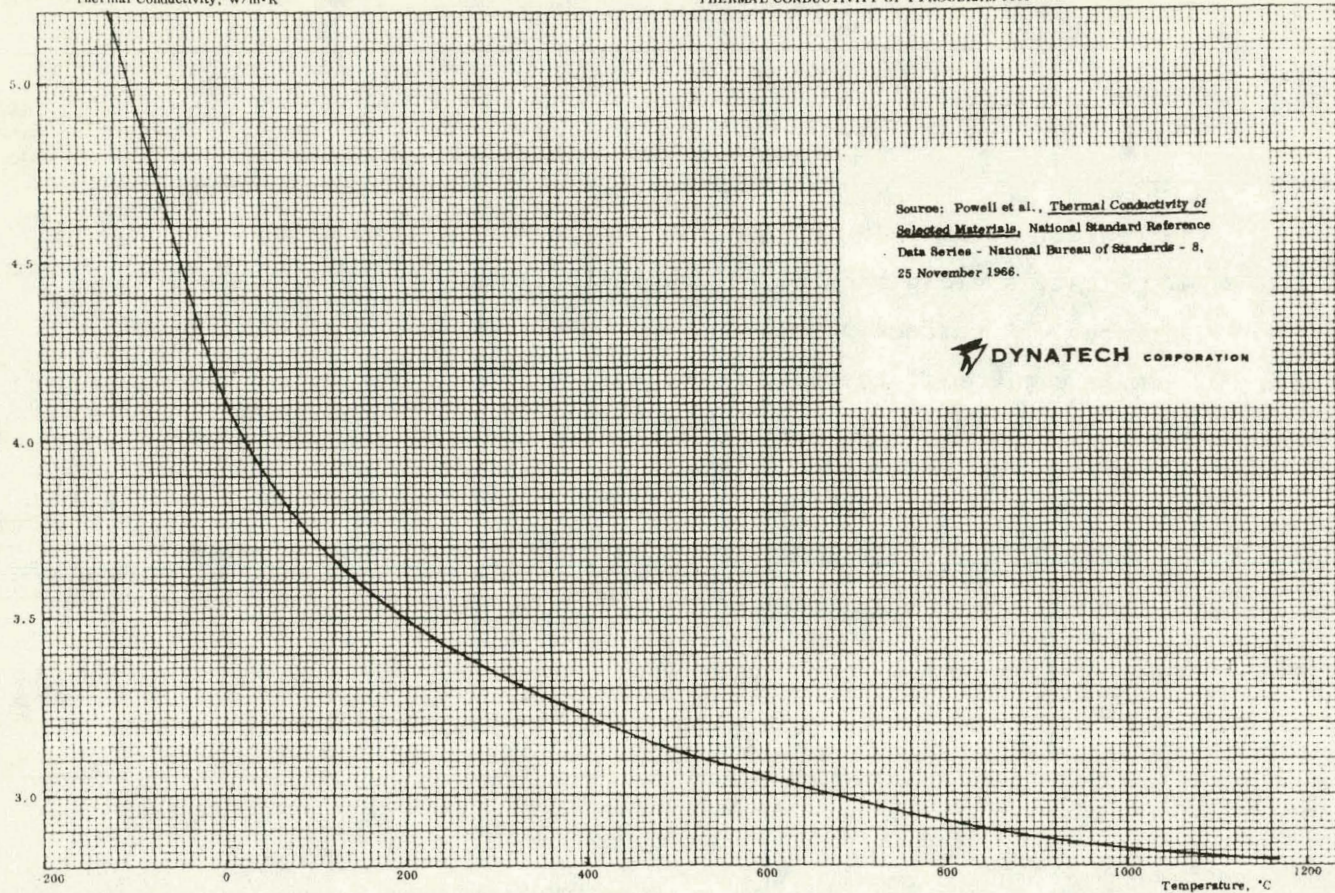
The contact resistance between the sample and references is controlled in two ways. First, a close machine tolerance is required of the sample and reference surfaces. A surface parallelness of 0.025 mm and a surface finish of  $3 \times 10^{-4}$  mm is required if possible. Second, the stack is loaded hydraulically to further reduce the contact resistances.

The two references which were used were Pyrex 7740 and Pyroceram 9606. These references closely matched the sample thermal conductivities. The thermal conductivities versus temperature for these materials is shown in Figures 4 and 5.



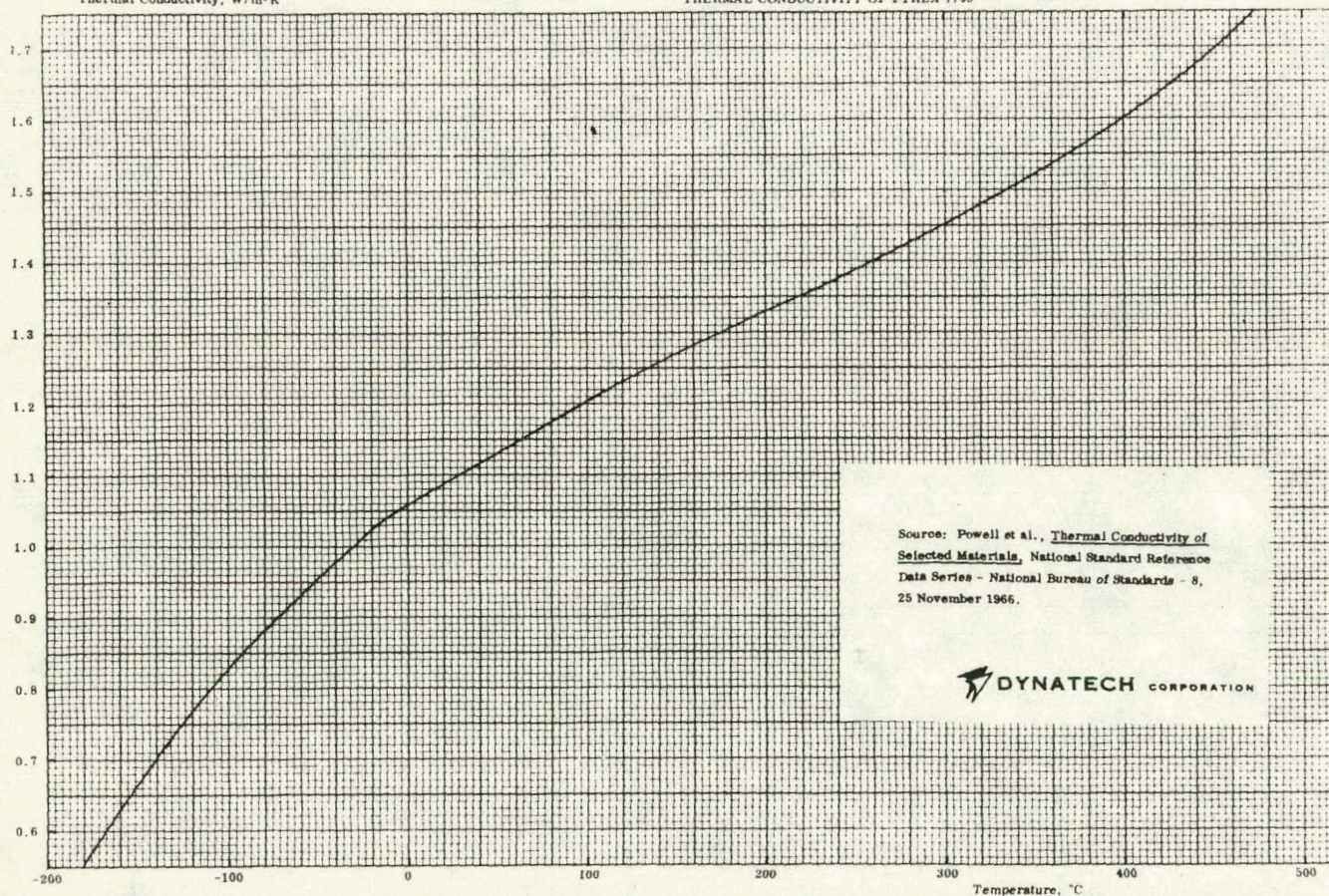
Thermal Conductivity, W/m·K

THERMAL CONDUCTIVITY OF PYROCERAM 9606



Thermal Conductivity, W/m·K

THERMAL CONDUCTIVITY OF PYREX 7740





#### 4. Experimental Procedure

The sample was removed from the dry desiccator just prior to test. The dimension of the samples were measured to the nearest 0.01 mm and the sample weighed to the nearest 0.01 g. Temperature sensors, Type K Chromel/Alumel thermocouples, were then cemented into the grooves using a ceramic cement. The sample was then placed into the test apparatus between the appropriate references, Pyrex 7740 or Pyroceram 9606. The heaters were adjusted to establish a 20K temperature difference across the specimen and a mean temperature of 300K  $\pm$  5K. Equilibrium conditions were established usually within one hour and data taken until calculations of the thermal conductivity over a period of one hour did not vary by more than 1%. From insertion in the stack to final equilibrium required approximately 3 hours. Once equilibrium was established, the heaters were raised to 400K and the procedure repeated until the last temperature, 700K was reached.

#### 5. Data Reduction

The data was reduced by computer and Data was then taken at 300, 400, 500, 600 and 700K from the smooth plot and tabulated as given in the following table.

#### 6. References

1. Francis, R. K., and Tinkelpaugh, J. R., J. Am. Ceram. Soc., 43, 560, 1960
2. Franci, J., and Kingery, W. D., J. Am. Ceram. Soc., 37, 80, 1954
3. Jakob, M., Heat Transfer, Vol I, 1949
4. Mirkovich, F. V., J. Am. Ceram. Soc., 48, 387, 1965
5. Morris R. D., and Hust, J. G., Phys. Res., 124, 1426, 1961
6. Stuckes, A. D., and Chasmar, R. P., Report on the Meeting on Semiconductors (Physical Society London), p. 119, 1965.
7. Thermal Conductivity, Vol. I, Ed. R. P. Tye, Academic Press, 1969, pp 174-182

Table  
THE THERMAL CONDUCTIVITY OF  
FIFTEEN SALT CORE SAMPLES

Sample Reference	Density $\text{kgm}^{-3}$	Thermal Conductivity $\text{W m}^{-1}\text{K}^{-1}$				
		300K	400K	500K	600K	700K
1A 2703.5-8 to 2704.7-8	2170	5.1	3.6	2.8	2.2	1.6
1B 2703.5-8 to 2704.7-8	2190	5.3	3.8	3.0	2.6	2.2
2 2055.3-8 to 2056-8	2070	5.2	3.8	3.1	2.5	2.0
3 ERDA 9/2840.7 to 2841.45	2910	4.7	3.6	3.0	2.7*	2.4*
4 ERDA 9/1908 to 1908.75	2210	4.8	3.5	2.6	1.95	1.65
5 ERDA 9/1910.3 to 1910.9	2580	1.45	1.15	0.95	0.85	0.75
6 ERDA 9/1631.4 to 1632	2870	4.3	3.9	3.2	2.6	2.3
7 ERDA 9/1086.8 to 1087.55	2120	5.3	3.8	2.8	2.2	1.6*
8 ERDA 9/1969.4 to 1970.1	2100	5.0	3.6	2.9	2.8	2.7*
9 AEC #8MB133/2001.9 to 2002.7	2770	3.0	1.95	1.4	1.15	0.95
10 AEC #8/1995.6 to 1996.1	2150	4.7	3.3	2.7	2.5	2.5 <sup>A</sup>
11 AEC #8/698 to 698.5	2300	1.95	.90	.50	.43	.40
12 AEC #8/1212.25 to 1213.1	2040	4.1	2.8	2.2	1.8	1.5
13 AEC #8/2062.6 to 2063.2	2080	4.9	3.6	2.9	2.5	2.1
14 WIPP19/616 to 617	2300	0.50	0.49	0.48	0.48	0.47
15 WIPP19/267.35 to 268.35	2550	2.6	2.2	1.9	1.7	1.6

\* Data extrapolated because samples disintegrated before temperature was reached.

DYNATECH R/D COMPANY TEL. 617-868-8050  
99 ERIE STREET • CAMBRIDGE, MA 02139 • USA



April 2, 1979

Mr. Jim McCreight  
Sandia Laboratories  
Albuquerque, NM 87115

Your Reference: Contract No. 13-0164  
Our Reference: SAD-15

Dear Jim:

The following table serves as the instrument calibration and verification for the salt core thermal conductivity measurement program. Most of the samples were similar in thermal conductivity to Pyroceram 9606, thus, Pyroceram 9606 was measured against Pyrex 7740. The following table indicates the actual measured thermal conductivity and the thermal conductivity as traceable to "Thermal Conductivity of Selected Materials", Powell et al., National Standard Reference Data Series - National Bureau of Standards - 8, 25 November 1966.


DYNATECH

Table

Temperature		Thermal Conductivity $W m^{-1} K^{-1}$		
C	K	Measured	Actual	% Error
36	309	3.7	3.95	-6
139	412	3.45	3.6	-4
238	511	3.35	3.45	-3
339	612	3.3	3.3	0
439	712	3.25	3.2	+1

If you have any questions, please do not hesitate to call.

Sincerely,

  
Stewart C. Spinney, Manager  
Thermophysical Properties Testing

ECS/wml

DYNATECH R/D COMPANY TEL. 617-868-8050  
99 ERIE STREET • CAMBRIDGE, MA 02139 • USA



August 6, 1979

Mr. Jim McCreight  
Sandia Laboratories  
Albuquerque, New Mexico 87115

Your Reference: Contract No. 13-0164  
Our Reference: SAD-15

Dear Jim:

Enclosed you will find two copies of our report on the linear thermal expansion of the salt and rock core specimens. The following table gives the thermal conductivity data on the last salt sample which you submitted, designated NaCl.

Sample Reference	Density kgm <sup>-3</sup>	Thermal Conductivity Wm <sup>-1</sup> K <sup>-1</sup>				
		300K	400K	500K	600K	700K
16 Salt NaCl	1,990	4.6	3.1	2.4	1.9	1.5

This completes the program. I look forward to discussing these results with you this fall when I visit to discuss the Comparative Instrument.

Sincerely,

A handwritten signature in dark ink, appearing to read "Stewart C. Spinney". The signature is fluid and cursive, with a large, sweeping flourish at the end.

Stewart C. Spinney  
Manager  
Thermophysical Properties Testing

SCS:tab  
Enclosures

Distribution:

U.S. Department of Energy, Headquarters  
Office of Nuclear Waste Management  
Washington, DC 20545

Eugene F. Beckett, Project Coordinator (WIPP) (1)  
Colin A. Heath, Director, Division of Waste Isolation (2)  
Sheldon Meyers  
Raymond G. Romatowski  
R. Stein  
Carl L. Cooley  
R. B. Chitwood

U.S. Department of Energy, Albuquerque Operations  
P.O. Box 5400  
Albuquerque, NM 87185

D. T. Schueler, Manager, WIPP Project Office (2)  
R. Rudolph, Acting Deputy Manager, WIPP Project Office  
G. Dennis, Director, Public Affairs Division  
S. C. Taylor, C&TI Division (for Public Reading Rooms)  
J. F. Bresson  
G. W. Johnson, Waste Management Branch

U.S. Department of Energy  
Carlsbad WIPP Project Office  
Room 113, Federal Building  
Carlsbad, NM 88220

U.S. Department of Energy  
c/o Battelle  
Office of Nuclear Waste Isolation  
505 King Avenue  
Columbus, OH 43201  
Jeff O. Neff

Battelle Memorial Institute  
Office of Nuclear Waste Isolation  
505 King Avenue  
Columbus, OH 43201  
Neil Carter, General Manager (3)  
R. Heineman  
Wayne Carbiener  
P. Hoffman  
A. A. Bauer

Westinghouse Electric Corporation  
P.O. Box 40039  
Albuquerque, NM 87196  
R. C. Mairson  
D. Hulbert  
V. F. Likar  
H. H. Irby  
A. K. Kuhn, D'Appolonia

National Academy of Sciences  
Committee on Radioactive Waste Management  
2101 Constitution Avenue  
Washington, DC 20418

---

J. Holloway (2)

Hobbs Public Library  
509 N. Ship Street  
Hobbs, NM 88248

---

Ms. Marcia Lewis, Librarian

Lokesh Chaturvedi  
Department of Civil Engineering  
Box 3E  
New Mexico State University  
Las Cruces, NM 88003

Bechtel Inc.  
P. O. Box 3965  
San Francisco, CA 94119

---

R. A. Langley  
H. G. Taylor  
D. L. Roberts  
D. Duncan

National Academy of Sciences, WIPP Panel

Frank L. Parker, Chairman  
Department of Environmental and  
Water Resources Engineering  
Vanderbilt University  
Nashville, TN 37235

Konrad B. Krauskopf, Vice Chairman  
Department of Geology  
Stanford University  
Stanford, CA 94305

Neville G. W. Cook, Member  
Dept. of Material Sciences and Engineering  
University of California at Berkeley  
Heart Mining Building, #320  
Berkeley, CA 94720

Merril Eisenbud, Member  
Inst. of Environmental Medicine  
New York University Medical Center  
Box 817  
Tuxedo, NY 10987

Fred M. Ernsberger, Member  
Glass Research Center  
PPG Industries, Inc.  
Box 11472  
Pittsburgh, PA 15238

Roger Kasperson, Member  
Center for Technology, Environment  
and Development  
Clark University  
Worcester, MA 01610

Richard R. Parizek, Member  
Department of Hydrogeology  
Pennsylvania State University  
University Park, PA 16802

Thomas H. Pigford, Member  
Department of Nuclear Engineering  
University of California  
Berkeley, CA 94720

National Academy of Sciences, WIPP Panel

Roger W. Staehle, Member  
Dean, Institute of Technology  
University of Minnesota  
Lind Hall  
Minneapolis, MN 55455

John W. Winchester, Member  
Department of Oceanography  
Florida State University  
Tallahassee, FL 32306

D'Arcy A. Shock, Consultant  
233 Virginia  
Ponca City, OK 74601

John T. Holloway, Executive Secretary  
2101 Constitution Avenue, NW  
Washington, DC 20418

WIPP Public Reading Room  
Atomic Museum, Kirtland East AFB  
Albuquerque, NM 87185

Ms. Gwynn Schreiner

WIPP Public Reading Room  
Carlsbad Municipal Library  
101 S. Hallagueno St.  
Carlsbad, NM 88220

Lee Hubbard, Head Librarian

Thomas Brannigan Library  
106 W. Hadley St.  
Las Cruces, NM 88001

Don Dresp, Head Librarian



Roswell Public Library  
301 N. Pennsylvania Avenue  
Roswell, NM 88201

---

Ms. Nancy Langston

Dr. Bruno Giletti, Co-Chairman  
Department of Geological Sciences  
Brown University  
Providence, Rhode Island 02912

Dr. Raymond Siever, Co-Chairman  
Department of Geological Sciences  
Harvard University  
Cambridge, Massachusetts 02138

Dr. John Handin, Director  
Center of Tectonophysics  
Texas A & M University  
College Station, Texas 77840

Dr. John Lyons  
Department of Earth Sciences  
Dartmouth College  
Hanover, New Hampshire 03755

Dr. George Pinder  
Department of Civil Engineering  
Princeton University  
Princeton, New Jersey 08540

New Mexico Advisory Committee on WIPP  
NMIMT Graduate Office  
Socorro, NM 87801

---

Marvin H. Wilkening, Chairman (2)

State of New Mexico  
Environmental Evaluation Group  
320 Marcy Street  
P.O. Box 968  
Santa Fe, NM 87503

---

Robert H. Neill, Director (2)

NM Department of Energy & Minerals  
P.O. Box 2770  
Santa Fe, NM 87501

---

Larry Kehoe, Secretary  
Kasey LaPlante, Librarian

J. E. Magruder  
Sandia Carlsbad Representative  
401 North Canal Street  
Carlsbad, NM 88220

Paul W. Levy  
Physics Department  
Brookhaven National Laboratory  
Associated Universities, Inc.  
Upton, Long Island, New York 11973

Sandia Internal

3141 T. L. Werner (5)  
3151 W. L. Garner, for: DOE/TIC (Unlimited Release) (3)  
3154-3 R. P. Campbell, for: DOE/TIC (25)  
4500 E. H. Beckner  
4510 W. D. Weart  
4511 D. W. Powers  
4512 T. O. Hunter (5)  
4512 C. L. Christensen  
4512 D. R. Fortney  
4512 M. A. Molecke  
4514 M. L. Merritt  
4530 R. W. Lynch  
4540 M. L. Kramm  
4541 L. W. Scully  
4542 Sandia WIPP Central Files (2)(TSI)  
4732 D. E. Munson  
5510 D. B. Hayes  
5511 J. W. Nunziato  
5511 D. F. McVey  
5511 G. R. Hadley  
5521 S. W. Key  
5530 W. Herrmann  
5531 S. W. Key  
5532 B. M. Butcher  
5800 R. S. Claassen  
Attn: 5810 R. G. Kepler  
5830 M. J. Davis  
5840 N. J. Magnani  
5820 R. E. Whan  
5824 J. N. Sweet (4)  
5824 J. E. McCreight (2)  
5824 J. A. Koski  
5824 M. Moss  
8310 D. M. Schuster  
8266 E. A. Aas (1)

[illegible]